International Journal of Physical Sciences

Volume 8 Number 31 23 August, 2013

ISSN 1992-1950

Academic Journals

ABOUT IJPS

The **International Journal of Physical Sciences (IJPS)** is published weekly (one volume per year) by Academic Journals.

International Journal of Physical Sciences (IJPS) is an open access journal that publishes high-quality solicited and unsolicited articles, in English, in all Physics and chemistry including artificial intelligence, neural processing, nuclear and particle physics, geophysics, physics in medicine and biology, plasma physics, semiconductor science and technology, wireless and optical communications, materials science, energy and fuels, environmental science and technology, combinatorial chemistry, natural products, molecular therapeutics, geochemistry, cement and concrete research, metallurgy, crystallography and computer-aided materials design. All articles published in IJPS are peer-reviewed.

Submission of Manuscript

Submit manuscripts as e-mail attachment to the Editorial Office at: ijps@academicjournals.org. A manuscript number will be mailed to the corresponding author shortly after submission.

For all other correspondence that cannot be sent by e-mail, please contact the editorial office (at ijps@academicjournals.org).

The International Journal of Physical Sciences will only accept manuscripts submitted as e-mail attachments.

Please read the **Instructions for Authors** before submitting your manuscript. The manuscript files should be given the last name of the first author.

Editorial Board

Instructions for Author

Electronic submission of manuscripts is strongly encouraged, provided that the text, tables, and figures are included in a single Microsoft Word file (preferably in Arial font).

The **cover letter** should include the corresponding author's full address and telephone/fax numbers and should be in an e-mail message sent to the Editor, with the file, whose name should begin with the first author's surname, as an attachment.

Article Types

Three types of manuscripts may be submitted:

Regular articles: These should describe new and carefully confirmed findings, and experimental procedures should be given in sufficient detail for others to verify the work. The length of a full paper should be the minimum required to describe and interpret the work clearly.

Short Communications: A Short Communication is suitable for recording the results of complete small investigations or giving details of new models or hypotheses, innovative methods, techniques or apparatus. The style of main sections need not conform to that of full-length papers. Short communications are 2 to 4 printed pages (about 6 to 12 manuscript pages) in length.

Reviews: Submissions of reviews and perspectives covering topics of current interest are welcome and encouraged. Reviews should be concise and no longer than 4-6 printed pages (about 12 to 18 manuscript pages). Reviews are also peer-reviewed.

Review Process

All manuscripts are reviewed by an editor and members of the Editorial Board or qualified outside reviewers. Authors cannot nominate reviewers. Only reviewers randomly selected from our database with specialization in the subject area will be contacted to evaluate the manuscripts. The process will be blind review.

Decisions will be made as rapidly as possible, and the journal strives to return reviewers' comments to authors as fast as possible. The editorial board will re-review manuscripts that are accepted pending revision. It is the goal of the IJPS to publish manuscripts within weeks after submission.

Regular articles

All portions of the manuscript must be typed double-spaced and all pages numbered starting from the title page.

The Title should be a brief phrase describing the contents of the paper. The Title Page should include the authors' full names and affiliations, the name of the corresponding author along with phone, fax and E-mail information. Present addresses of authors should appear as a footnote.

The Abstract should be informative and completely self-explanatory, briefly present the topic, state the scope of the experiments, indicate significant data, and point out major findings and conclusions. The Abstract should be 100 to 200 words in length.. Complete sentences, active verbs, and the third person should be used, and the abstract should be written in the past tense. Standard nomenclature should be used and abbreviations should be avoided. No literature should be cited.

Following the abstract, about 3 to 10 key words that will provide indexing references should be listed.

A list of non-standard **Abbreviations** should be added. In general, non-standard abbreviations should be used only when the full term is very long and used often. Each abbreviation should be spelled out and introduced in parentheses the first time it is used in the text. Only recommended SI units should be used. Authors should use the solidus presentation (mg/ml). Standard abbreviations (such as ATP and DNA) need not be defined.

The Introduction should provide a clear statement of the problem, the relevant literature on the subject, and the proposed approach or solution. It should be understandable to colleagues from a broad range of scientific disciplines.

Materials and methods should be complete enough to allow experiments to be reproduced. However, only truly new procedures should be described in detail; previously published procedures should be cited, and important modifications of published procedures should be mentioned briefly. Capitalize trade names and include the manufacturer's name and address. Subheadings should be used. Methods in general use need not be described in detail.

Results should be presented with clarity and precision. The results should be written in the past tense when describing findings in the authors' experiments. Previously published findings should be written in the present tense. Results should be explained, but largely without referring to the literature. Discussion, speculation and detailed interpretation of data should not be included in the Results but should be put into the Discussion section.

The Discussion should interpret the findings in view of the results obtained in this and in past studies on this topic. State the conclusions in a few sentences at the end of the paper. The Results and Discussion sections can include subheadings, and when appropriate, both sections can be combined.

The Acknowledgments of people, grants, funds, etc should be brief.

Tables should be kept to a minimum and be designed to be as simple as possible. Tables are to be typed double-spaced throughout, including headings and footnotes. Each table should be on a separate page, numbered consecutively in Arabic numerals and supplied with a heading and a legend. Tables should be self-explanatory without reference to the text. The details of the methods used in the experiments should preferably be described in the legend instead of in the text. The same data should not be presented in both table and graph form or repeated in the text.

Figure legends should be typed in numerical order on a separate sheet. Graphics should be prepared using applications capable of generating high resolution GIF, TIFF, JPEG or Powerpoint before pasting in the Microsoft Word manuscript file. Tables should be prepared in Microsoft Word. Use Arabic numerals to designate figures and upper case letters for their parts (Figure 1). Begin each legend with a title and include sufficient description so that the figure is understandable without reading the text of the manuscript. Information given in legends should not be repeated in the text.

References: In the text, a reference identified by means of an author‘s name should be followed by the date of the reference in parentheses. When there are more than two authors, only the first author‘s name should be mentioned, followed by ’et al‘. In the event that an author cited has had two or more works published during the same year, the reference, both in the text and in the reference list, should be identified by a lower case letter like ’a‘ and ’b‘ after the date to distinguish the works.

Examples:

Abayomi (2000), Agindotan et al. (2003), (Kelebeni, 1983), (Usman and Smith, 1992), (Chege, 1998; 1987a,b; Tijani, 1993,1995), (Kumasi et al., 2001)

References should be listed at the end of the paper in alphabetical order. Articles in preparation or articles submitted for publication, unpublished observations, personal communications, etc. should not be included in the reference list but should only be mentioned in the article text (e.g., A. Kingori, University of Nairobi, Kenya, personal communication). Journal names are abbreviated according to Chemical Abstracts. Authors are fully responsible for the accuracy of the references.

Examples:

Ogunseitan OA (1998). Protein method for investigating mercuric reductase gene expression in aquatic environments. Appl. Environ. Microbiol. 64:695-702.

Gueye M, Ndoye I, Dianda M, Danso SKA, Dreyfus B (1997). Active N2 fixation in several Faidherbia albida provenances. Ar. Soil Res. Rehabil. 11:63-70.

Charnley AK (1992). Mechanisms of fungal pathogenesis in insects with particular reference to locusts. In: Lomer CJ, Prior C (eds) Biological Controls of Locusts and Grasshoppers: Proceedings of an international workshop held at Cotonou, Benin. Oxford: CAB International, pp 181-190.

Mundree SG, Farrant JM (2000). Some physiological and molecular insights into the mechanisms of desiccation tolerance in the resurrection plant Xerophyta viscasa Baker. In Cherry et al. (eds) Plant tolerance to abiotic stresses in Agriculture: Role of Genetic Engineering, Kluwer Academic Publishers, Netherlands, pp 201-222.

Short Communications

Short Communications are limited to a maximum of two figures and one table. They should present a complete study that is more limited in scope than is found in full-length papers. The items of manuscript preparation listed above apply to Short Communications with the following differences: (1) Abstracts are limited to 100 words; (2) instead of a separate Materials and Methods section, experimental procedures may be incorporated into Figure Legends and Table footnotes; (3) Results and Discussion should be combined into a single section.

Proofs and Reprints: Electronic proofs will be sent (e-mail attachment) to the corresponding author as a PDF file. Page proofs are considered to be the final version of the manuscript. With the exception of typographical or minor clerical errors, no changes will be made in the manuscript at the proof stage.

International Journal of Physical Sciences

Table of Contents: Volume 8 Number 31 23 August, 2013

ARTICLES

academicJournals

Vol. 8(31), pp. 1570-1580, 23 August, 2013
DOI: 10.5897/IJPS2013.3974
ISSN 1992 - 1950 © 2013 Academic Journals
http://www.academicjournals.org/IJPS

International Journal of Physical Sciences

Full Length Research Paper

Optical properties of as-deposited TiO_2 thin films prepared by DC sputtering technique

M. M. Abd El-Raheem[1,2] and Ateyyah M. Al-Baradi[1]

[1]Department of Physics, Faculty of Science, Taif University, Taif 888, Saudi Arabia.
[2]Department of Physics, Faculty of Science, Sohag University, Sohag 82524, Egypt.

Accepted 8 August, 2013

Amorphous titanium dioxide TiO_2 thin films have been deposited using the dc sputtering technique. The structure of the films was analyzed by X-ray diffraction and the results showed non-crystalline behavior. The optical properties of these thin films have been investigated by means of optical reflectance and transmittance spectra. The optical energy gap E_g, the Urbach tails E_u, the single oscillator energy E_o, the dispersion energy E_d and the optical constants as refractive index n, extinction coefficient k dielectric constant and optical conductivity were estimated.

Key words: Titanium dioxide, optical energy gap, refractive index, oscillator energy, dispersion energy.

INTRODUCTION

Titanium dioxide TiO_2 thin films are the most widely used coatings due to their desirable properties, such as good adhesion, high stability against mechanical abrasion, chemical attach, and high temperature (Pulker, 1984; Ritter, 1975). Therefore, they are used as single-layer or multilayer optical coatings (Macleon, 1986). Titanium dioxide thin films have been largely studied as photo anodes in the process of photo electrolysis of water in solar energy conversion systems, electrochromic materials for display devices, smart windows, antireflective coatings, optical filters (Yoko, et al., 1988; Doeuff et al., 1986; Livage, 1986; Nabavi et al., 1989; Dislich and Hinz, 1982). Titanium dioxide films can be prepared using different kind of methods: thermal or anodic oxidation of titanium, electron beam evaporation, ion sputtering, chemical vapour deposition and sol-gel method (Yoldas, 1980; Henry, 1978; Lottiaux et al., 1989; Babuji et al., 1983; Yeung and Lam, 1983; Ozer et al., 1992; Yun et al., 2003). It was reported that titanium dioxide exists in three different phases: anatase, rutile, and brookite. Only anatase, rutile and amorphous film have been observed in TiO_2 thin films up to now (Lo¨ et al., 1994). TiO_2 film in anatase phase has a variety of application prospects in the field of environmental protection (Dumitriu, et al., 2000; Takeda et al., 2001). The rutile structure of TiO_2 thin film is known as a good blood compatibility material and can be used as artificial heart valves (Zhang et al., 1996). Much technique was used to achieve TiO_2 thin film (Takeda et al., 2001; Watanabe et al., 2000). Magnetron sputtering is one of the most easily to industrialize, and to achieve the high quality thin film in large area substrates (Dumitriu et al., 2000; Treichel and Kirchhoff, 2000). Mid-frequency ac magnetron sputtering using pure titanium target was

*Corresponding author. E-mail: elneh@yahoo.com.

PACS. 78.20.Ci optical constants.

studied widely (Bra¨uer et al., 1998; Hou et al., 2000). The optical constants of TiO_2 thin films were studied using spectroscopic ellipsometry.

The aim of the present work is to prepare thin films of TiO_2 using dc sputtering technique and to study their optical properties with change in their thicknesses.

EXPERIMENTAL TECHNIQUE

Titanium dioxide TiO_2 thin layers were prepared by DC sputtering under a base pressure (95% argon + 5% O_2) of 15 mTorr. TiO_2 target (from Cathey) with a purity of 99.998% and 3 inch diameter was used. The target-substrate distance was fixed at 11 cm. For obtaining homogeneous films, periodic motion of 2 rpm of the substrates was adopted. Thin films of TiO_2 were deposited on a pre-cleaned glass substrate using UNIVEX 350 sputtering unit with dc power model Turbo drive TD20 classic (Lybold) and rate thickness monitor model INFICON AOM-160. The structural characteristics of TiO_2 thin films were investigated by X-ray diffraction pattern. Philips X-ray diffractometer model X' Pert was used for the measurements which utilized monochromatic CuKα = 1.5406 Å radiation operated at 40 kV and 25 mA.

Reflectance R and transmittance T measurements under near-normal incidence in the spectral range 200-1000 nm were performed by using double beam spectrophotometer (JASCO model V-670 UV-VIS-NIR). The substrate temperature was kept at 25°C during deposition. In this paper, we report on the optical properties of amorphous TiO_2 thin films deposited by dc sputtering

Theory and calculations

For obtaining the optical energy gap E_{op}, the following equation was used (Pal et al., 1993):

$$(\alpha h\upsilon)^b = A(h\upsilon - E_{op}) \quad (1)$$

where the absorption coefficient α can be expressed as (Ali, 2005):

$$\alpha = \frac{1}{d} Ln\left(\frac{(1-R)^2}{T}\right) \quad (2)$$

The absolute value of transmittance T is given by (El-Nahass, 1992):

$$T = \left(\frac{I_{fr}}{I_g}\right)(1 - R_g) \quad (3)$$

$(h\nu)$ is the incident photon energy, R is the reflectance, R_g is the reflectance of glass substrate, I_{ft} is the intensity of light passing through the film-glass system, I_g is the intensity of the light passing through the reference glass and d is the film thickness. The absolute value of the reflectance R is given by (Bakry and El-Naggar, 2000):

$$R = [(\frac{I_{fr}}{I_m})R_m(1 + [1 - R_g]^2) - T^2 R_g \quad (4)$$

I_{fr} is the intensity of light reflected from the sample, I_m is the intensity of light reflected from the reference mirror.

The refractive index n was calculated from the following equation (El-Nahass et al., 2008):

$$n = \frac{1+R}{1-R} + [\frac{4R}{(R-1)^2} - k^2)]^{1/2} \quad (5)$$

where $k = \alpha\lambda / 4\pi$ is the absorption index, and λ the is incident wavelength.

The amount of tailing can be estimated to a first approximation by plotting the absorption edge data in terms of an equation originally given by Urbach (1953), which has been applied to many glassy materials. The exponential depends on the absorption coefficient, (α) and photon energy ($h\nu$). It has been found that $h\nu$ holds over several decades for a glassy material and takes the formula:

$$\alpha = \alpha_o e^{\frac{h\upsilon}{E_u}} \quad (6)$$

Using DiDomenico dispersion relationship (Wemple and DiDomenco, 1973), the single oscillator energy E_o and dispersion energy E_d can be calculated:

$$(n^2 - 1)^{-1} = \frac{E_o}{E_d} - \frac{1}{E_o E_d}(h\upsilon)^2 \quad (7)$$

For obtaining the lattice dielectric constant ε_L, the following equation is used (El-Nahass et al., 2010):

$$\varepsilon_1 = n^2 = \varepsilon_L - \frac{e^2 N}{4\pi\varepsilon_o m^* c^2}\lambda^2 \quad (8)$$

Where e is the elementary charge, ε_o is the permittivity of free space, N/m* is the ratio of free carrier concentration to the effective mass.

RESULTS AND DISCUSSION

Structural investigation

X-ray diffraction patterns of titanium dioxide TiO_2 thin films of as-prepared showed amorphous structure as shown in Figure 1 where the patterns did not include any peak representing crystallization.

Optical characterization

Effect of thickness of TiO_2 on the optical properties

Figure 2 depicts the changes of the transmittance T(%) with the incident wavelength. Throughout the range of the incident wavelength from 200 to 500 nm, there were peaks belonging to the films of thicknesses 100, 120, 150, 175 and 200 nm and had the values 60, 72, 83, 87, and 90% at 380, 380, 400, 405 and 425 nm, respectively. It can be noticed that the peaks of the transmittance were shifted toward a longer wavelength with increasing the thickness of the films as shown in Figure 2. The highest values of the transmittance were followed with decreasing their values with prolongating the wavelength for the considered thin films except for the film of thickness 100 nm. It can be noticed also that the

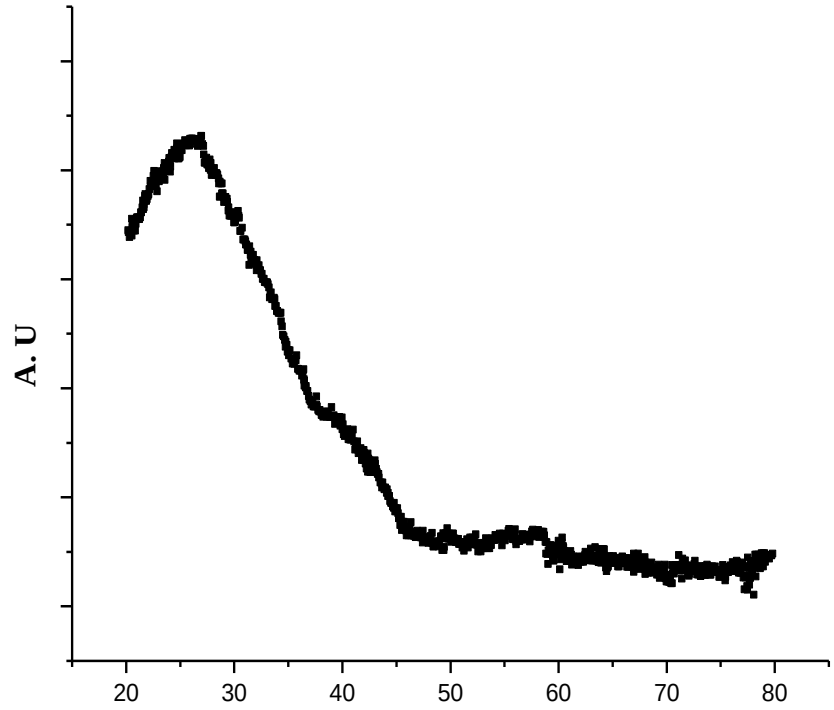

Figure 1. X-ray diffraction patterns of as0prepared $Ti0_2$ thin film.

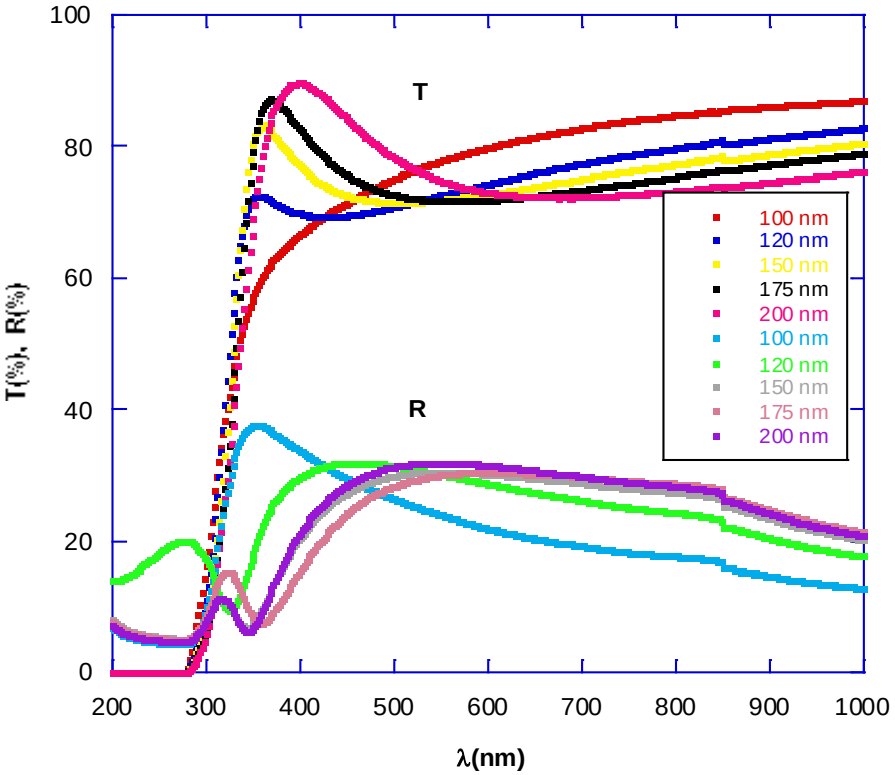

Figure 2. The optical transmittance T (λ) and reflectance R (λ) forthe as prepared TiO_2 thin films of different thicknesses.

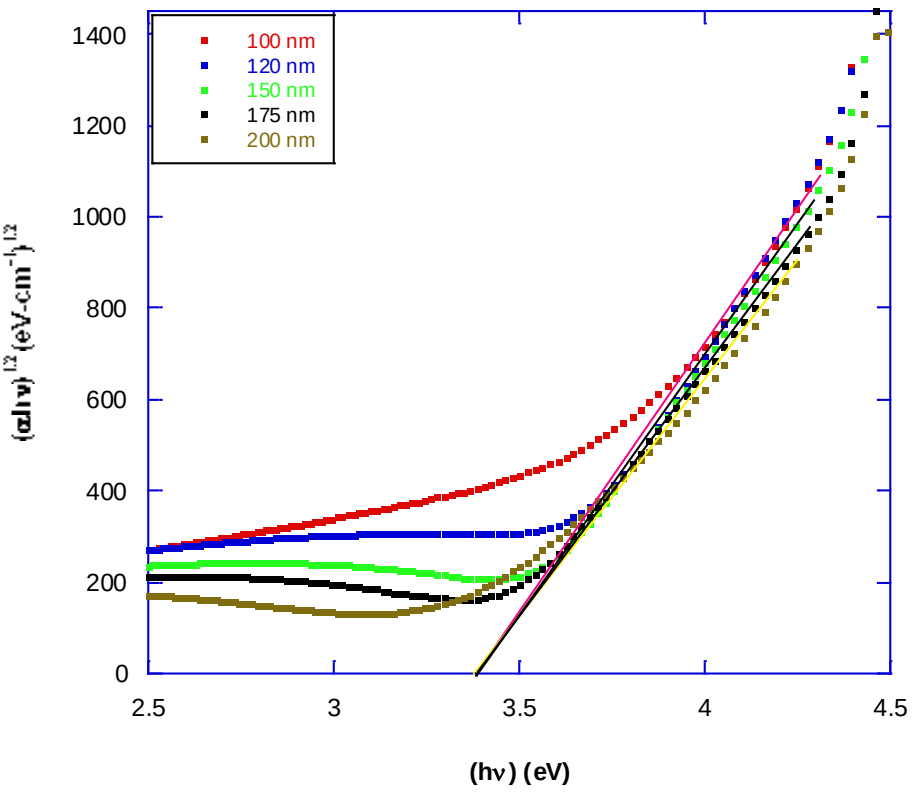

Figure 3. Plots of $(\alpha h\nu)^{1/2}$ vs. $h\nu$ for as-prepared TiO_2 thin films of different thicknesses.

transmittance decreases with increasing the film thickness which can be due to an increase in both reflection and absorption in the thin films (Al-Ofi et al., 2012). In addition, film structure may lose its homogeneity with increasing the film thickness due to accumulation of different types of structural faults, hence increasing film absorption. The transmittance loss at longer wavelengths results from photon-electron interaction, which can scatter the photons. This loss occurs from both reflection and absorption. Reflection in this range is not strictly a surface phenomenon (Robert et al., 2005). However, reflection from the bulk of the material can occur, provided that the photon escapes the surface. If the scattered photon does not escape the surface, it can be concluded to have been absorbed (Robert et al., 2005).

The results of reflectance verify the transmittance one as shown in Figure 2, where the reflectance increased in the region of decreasing the transmittance. On the other hand, the top of the transmittance were corresponding to the bottom of the transmittance. Figure 3 shows the relation $(\alpha h\upsilon)^{1/2}$ vs. $(h\upsilon)$ for as-prepared TiO_2 thin films with different thicknesses. The values of the allowed indirect optical energy gap E_{op} can be obtained from the plots of $(\alpha h\upsilon)^{1/2}$ versus $(h\upsilon)$ by extrapolating the linear portion of the plots of $(\alpha h\upsilon)^{1/2}$ versus $(h\upsilon)$ to $\alpha = 0.0$ as shown in Figure 3. The estimated values of the optical energy gap were found to be independent on the film thickness where it had the same value 3.36 eV for all the considered film thickness. This value 3.36 eV of the optical gap of the thin films under test is very close to the reported one 3.27 eV (Ya-Qi et al., 2003). The Urbach tails (width of the band tails of the localized states) represents the degree of disorder in an amorphous semiconductor E_u for as-prepared TiO_2 thin films can be obtained from the slopes of the straight lines of the plot Ln(α) versus $h\upsilon$ as shown in Figure 4. Results of Urbach tails confirmed the results of optical gap, where E_u was found to have the same value 0.37±eV within the experimental error for all the considered films (El-Raheem et al., 2012).

The variations of both the real part of the refractive index n and the extinction coefficient k with wavelength are shown in Figure 5. It is apparent that the refractive index decreases with increasing the incident wavelength in the visible range of frequency revealing the normal dispersion. Further, the refractive index increases with increasing the film thickness; this may be due to changing the film thickness which could change the density and/or the polarization of the material of the thin films. On the other hand, the variations of the extinction

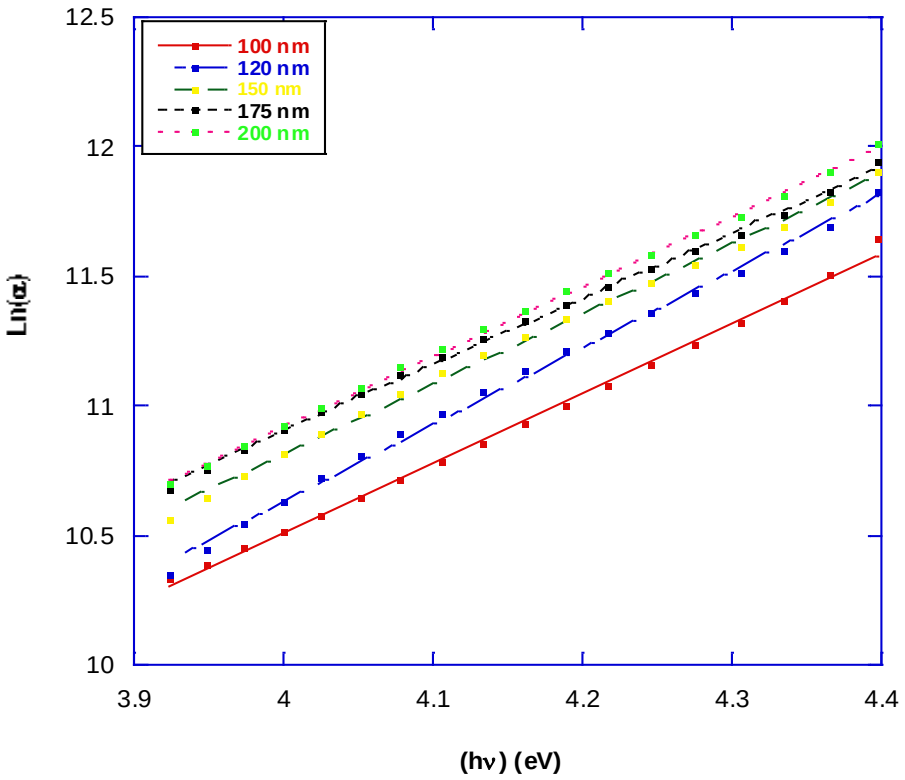

Figure 4. Plots of Ln(α) vs. photon energy for as-prepared TiO_2 thin films of different thicknesses.

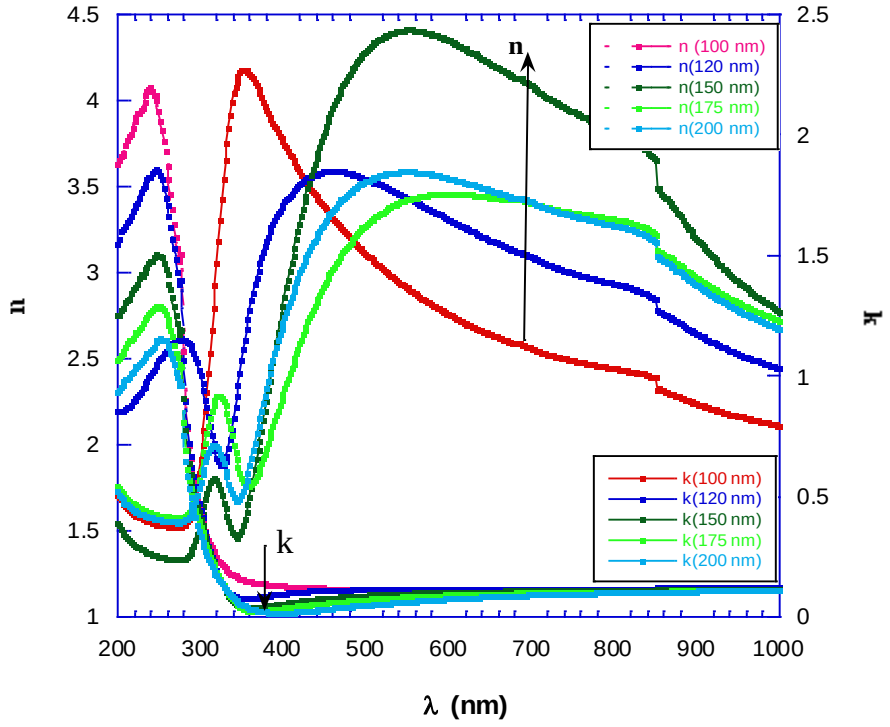

Figure 5. Spectra of the refractive index n and the extenction coefficiont k of TiO_2 thin films of different thicknesses.

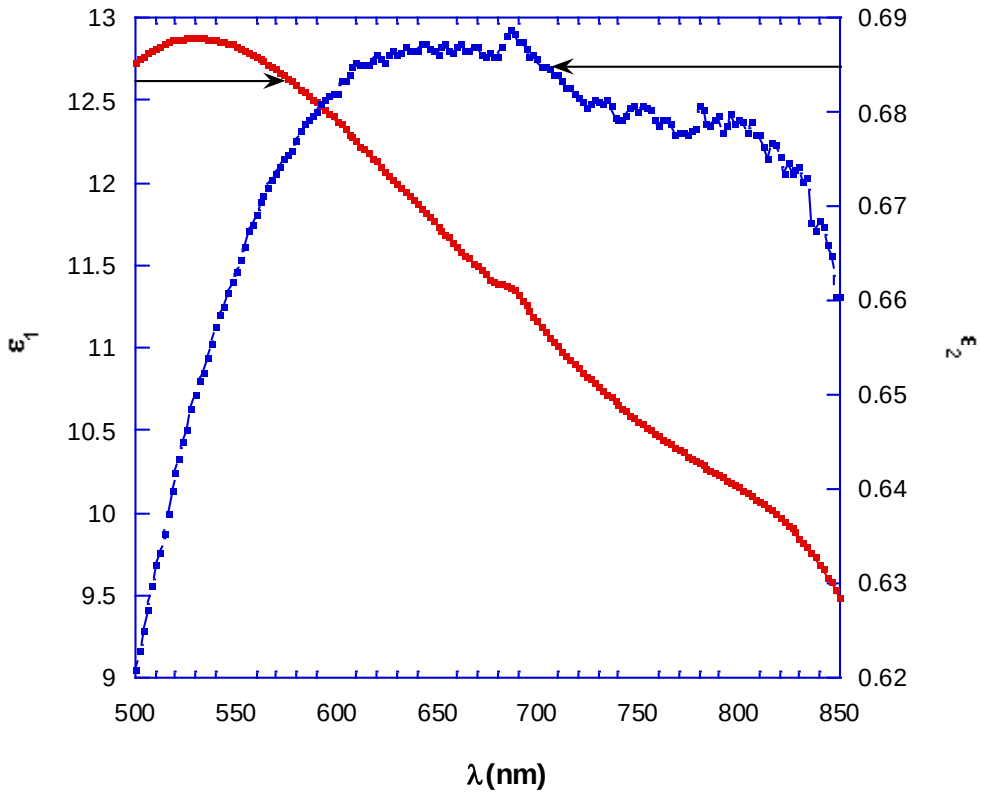

Figure 6. Variations of the average values of real and imaginary part of the dielectric function with incident wavelength.

coefficient k reverse the behavior of the refractive index. Figure 6 depicts the changes of both the average values (belonging to the different thicknesses of the thin films under test) real ε_1 and imaginary ε_2 parts of the dielectric function with incident wavelength. The real part of the dielectric constant relates to dispersion, whereas dissipative rate of the electromagnetic wave in the dielectric medium is provided by imaginary part. It is clear that the variations of ε_1 follows the same trend as the real part of the refractive index and the imaginary part ε_2 follows the behavior of the extinction coefficient k with the incident wavelength as shown in Figure 5. Figure 7 depicts the variations of the loss factor tan δ with wavelength indicating that the loss factor decreases sharply with increasing the wavelength within the range from 300 to 400 nm and the increases slightly. To calculate the real and imaginary components of optical conductivity the following equations are used (Caglar et al., 2007):

$$\sigma_1 = \omega\varepsilon_2\varepsilon_0 \text{ and } \sigma_2 = \omega\varepsilon_1\varepsilon_0$$

where ω is the angular frequency, ε_0 is the permittivity of free space. The spectra of real and imaginary parts of the optical conductivity are shown in Figure 8. It can be seen that both the real and imaginary part increases with increasing the photon energy up to 2.6 eV which can be attributed to excitation of electrons by photon energy (Caglar et al., 2007).

Real part of optical conductivity continue increasing sharply beyond 3.6 eV of photon energy as seen in Figure 8 suggesting strong excitation of the electrons. The volume energy loss function VELF and surface energy loss function SELF (volume and surface energy loss functions are proportional to the characteristic energy loss of fast electrons traveling the bulk and surface of the material, respectively) can be calculated using the following equations:

$$SELF = \frac{\varepsilon_2^2}{((\varepsilon_1+1)^2+\varepsilon_2^2)}$$

$$VELF = \frac{\varepsilon_2^2}{\varepsilon_1^2-\varepsilon_2^2}$$

The changes of VELF and SELF of as-prepared TiO_2 thin films with photon energy are shown in Figure 9; this change can be explained in terms of the response of a set of Lorentzian oscillators of adjustable strength and position (Ghanashyam et al., 1999). Wemple and DiDomenico (1973) introduced two parameters, the dispersion energy E_d which has a meaning of the

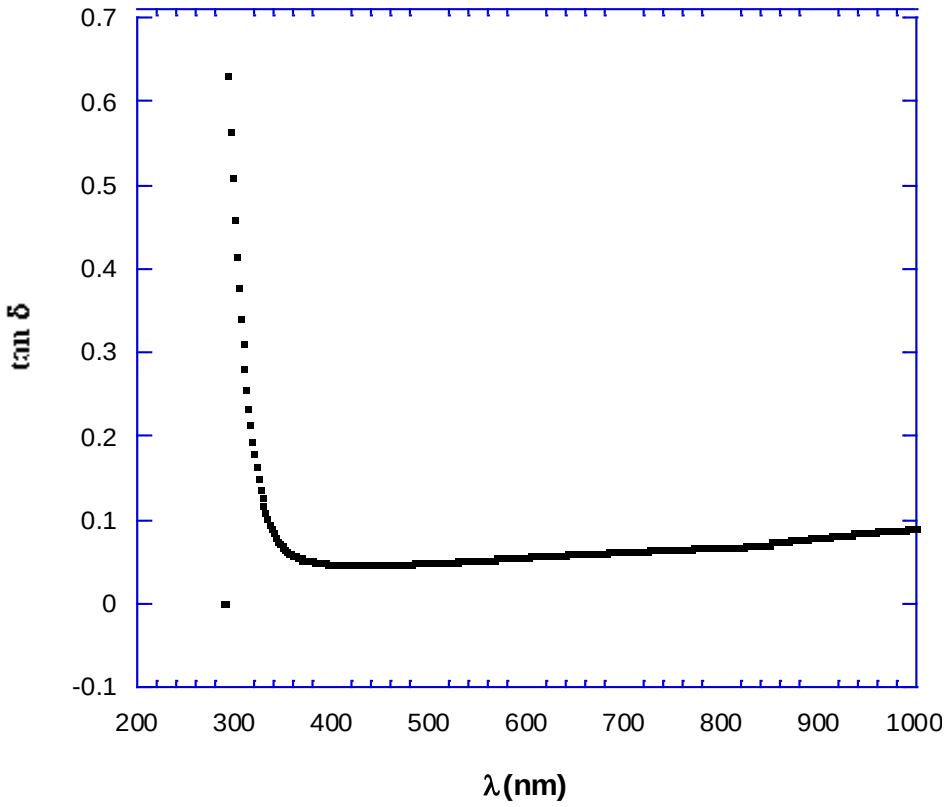

Figure 7. Variations of the loss factor δ with wavelength for TiO_2 thin films.

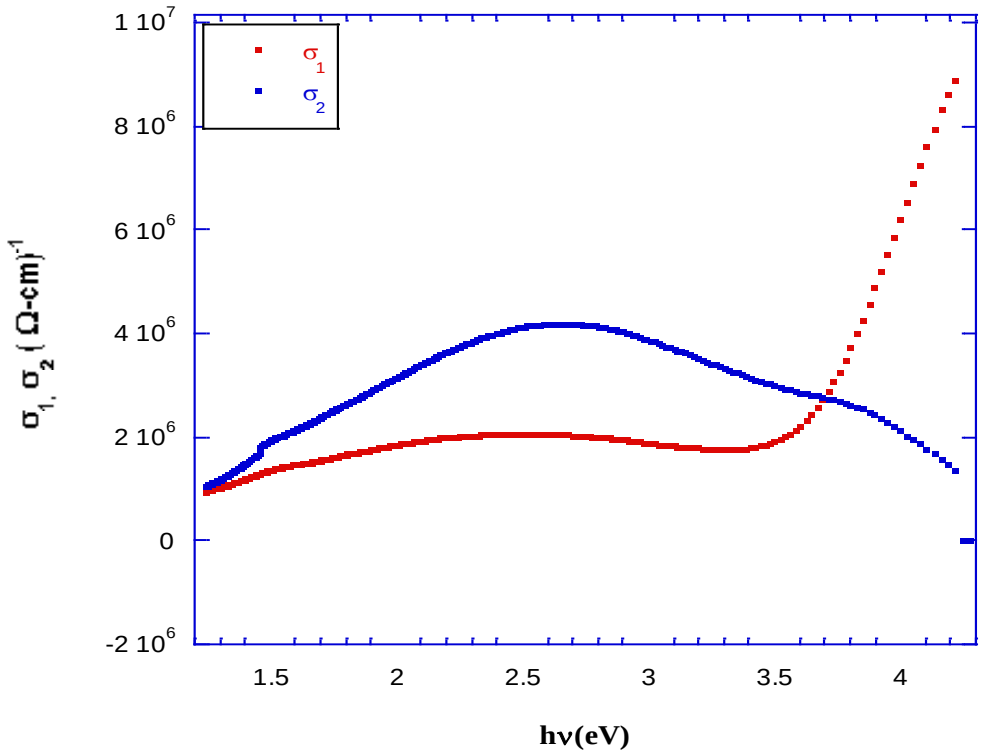

Figure 8. Spectra of the real and imaginary part of the optical conductivity of the TiO_2 thin films.

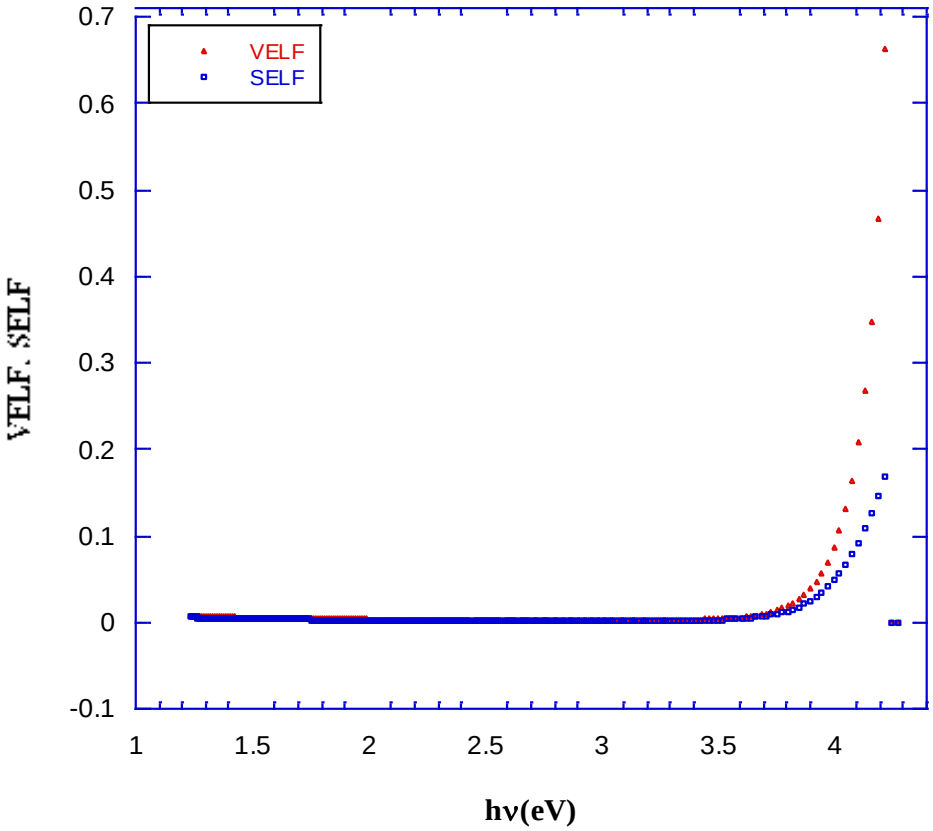

Figure 9. The distribution of the volume and surface energy loss for TiO_2 thin films as a function of thoton energy.

oscillator strength of the interband transition and describes the dispersion of the refractive index, and the single oscillator energy E_o which has a meaning of the average interband transition energy. Both of the two parameters can be calculated from the slope and intercept of Figure 10 and recorded in Table 1. The average value of the oscillator energy of the thin films under test is 3.486 eV which is in consistent to the optical energy gap estimated from Figure 3. This agree with Olomon et al. (1988) which reported that the single oscillator energy gives a quantitative information on the overall band structure of the material "average gap" and corresponds to the distance between the centers of gravity of the valence and conduction bands. The close value of the optical gap 3.36 eV and average value of single oscillator 3.486 eV is in good agreement with the relation reported by Timoumi et al. (2011). It is reported that the dispersion energy relates other physical parameters through the following empirical relationship (Wemple and DiDomenco, 1973; Timoumi et al., 2011):

$E_d = \beta N_c Z_a N_e$ (eV)

where N_c is the coordination number of the cation nearest – neighbor to the anion, Z_a is the formal chemical valency of the anion, N_e is the effective number of valence electrons per anion and β is a constant. Taking the experimental average value of E_d for the as deposited films (E_d=22.12 eV), Z_a = 2, N_c = 6, N_e = 6, then β = 0.31 eV, this leads to TiO_2 thin films under test fall into ionic class. The moments of the optical spectra M_{-1} and M_{-3} can be obtained from the relationship (Yakuphanoglu et al., 2004):

$$E_o^2 = \frac{M_{-1}}{M_{-3}} \quad , E_d^2 = \frac{M_{-1}^2}{M_{-3}}$$

It is found that the calculated values of the moments M_{-1} increase with increasing the thickness of the films, whereas the moments M_{-3} decrease. The ratio $(\frac{N}{m^*})$ and the lattice dielectric constant (the high frequency dielectric constant) ε_L for the thin films are calculated from Figure 11 which represents the plot of n^2 vs. λ^2 and then tabulated in Table 1. It can be noticed that both $(\frac{N}{m^*})$ and ε_L increases with increasing the thickness of the film from 100 to 150 nm.

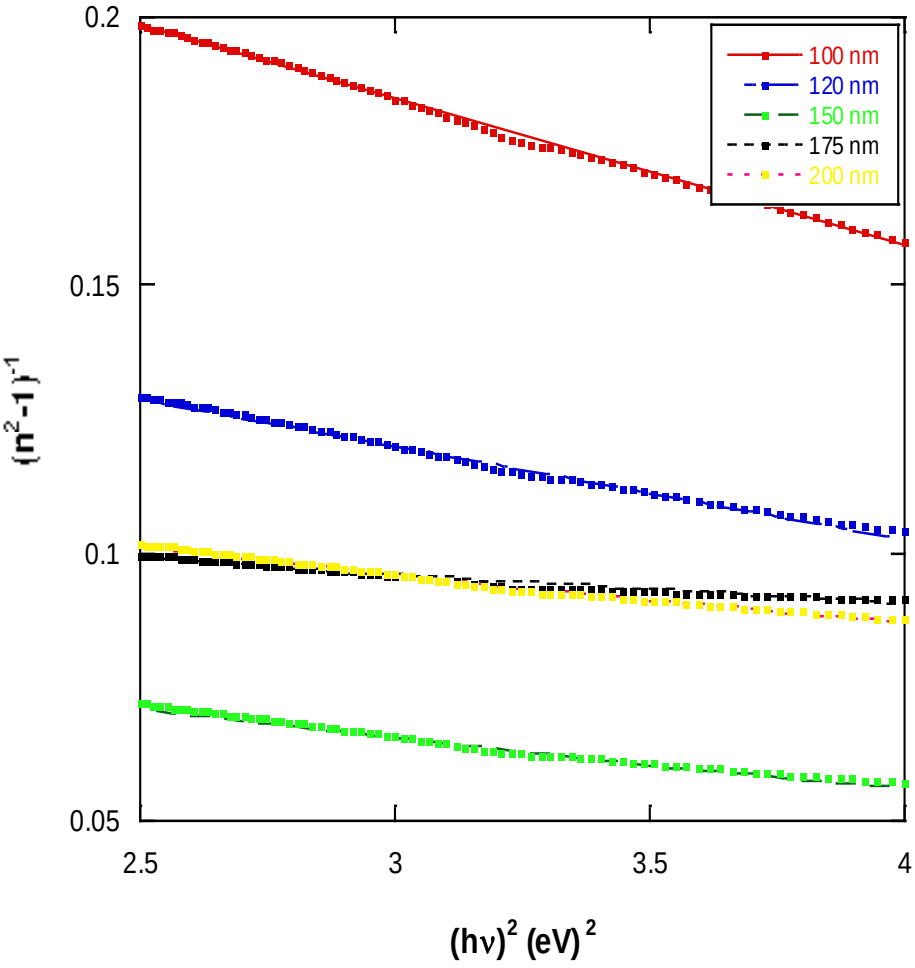

Figure 10. Plts of $(n^2 - 1)^{-1}$ vs. hν for as-prepared TiO_2 thin films of different thicknesses.

Table 1. The optical energy gap, Urbach energy, refractive index dispersion parameters of TiO_2 thin films.

Film thickness nm	E_g (eV)	E_u (eV)	E_o (eV)	E_d (eV)	β	M_{-1}	M_{-3} $(eV)^{-2}$	$(N/m^*)x10^{48}$ $(g^{-1}\ cm^{-3})$	ε_L
100	3.36	0.371	3.128	11.63	0.16	3.72	0.028	1.67	8.7
120	3.36	0.337	3.153	18.18	0.25	5.77	0.018	2.66	12.9
150	3.36	0.369	3.08	32.11	0.45	10.42	0.010	5.51	23.6
175	3.36	0.390	4.421	39.06	0.54	8.82	0.006	1.65	13.6
200	3.36	0.369	3.646	28.79	0.39	7.79	0.009	2.46	14.7

Conclusion

The optical properties of amorphous TiO_2 thin films under test showed that, changing the thickness of the films has not affected the optical energy gap and Urbach tails. The average value of the single oscillator energy has a value very close to that of the optical energy gap. The dispersion energy found to increase with increasing the thickness of the film, its average value used to estimate the value of β showing that TiO_2 under test is ionic. The moments M_{-1} showed an increase with thickness from 100 to 150 nm, whereas, the moments M_{-3} showed a decrease with thickness. Both $(\frac{N}{m^*})$ and ε_L showed an increase with thickness from 100 to 150 nm.

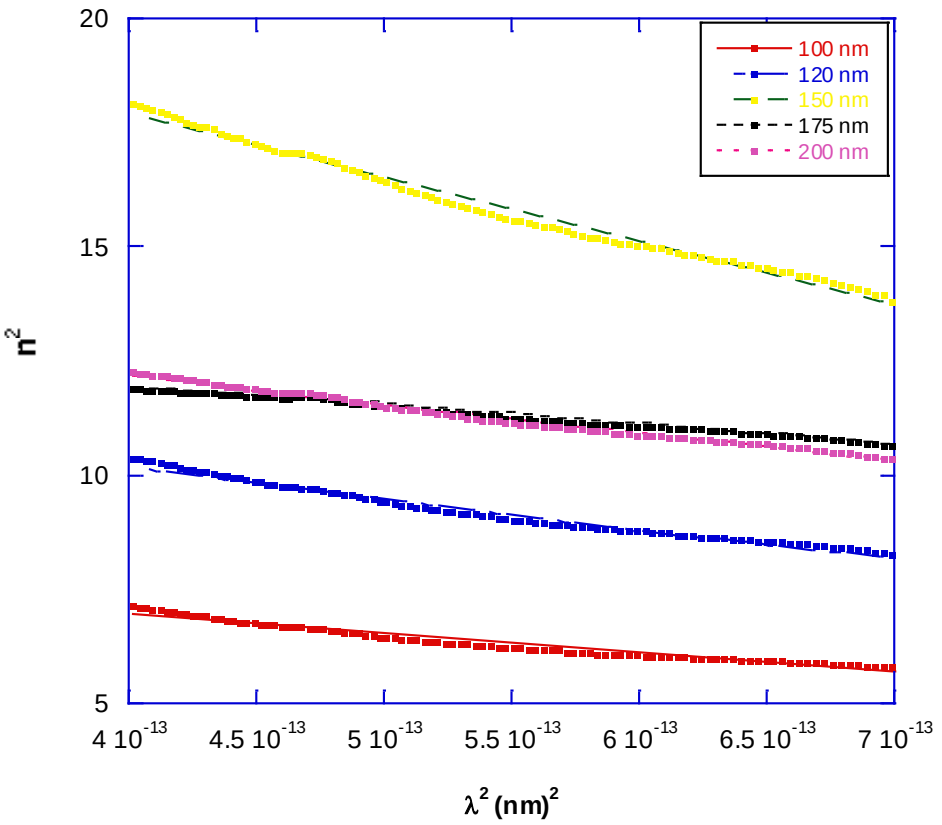

Figure 11. Plots of n^2 against λ^2 for as-prepared TiO_2 thin films of different thicknesses.

REFERENCES

Ali HM (2005). Characterization of a new transparent-conducting material of ZnO doped ITO thin films. Phys. Status Solidi A 202:2742-2752.

Al-Ofi' HH, Abd El-Raheem MM, Ateyyah M, Al-Baradi A, Atta A (2012). Structural And Optical Properties Of Al2zno4 Thin Films Deposited By Dc Sputtering Technique. J. Non-Oxide glasses 3:39-54.

Babuji B, Balasubramanian C, Radhakrishnan M (1983). Dielectric Properties Of Ion Plated Titanium Oxide Thin Films. J. Non-Crys. Solids 55:405-412.

Bakry AM, El-Naggar AH (2000). Doping Effects on the Optical Properties of Evaporated A-Si: H Films. Thin Solid Films pp. 360:293-297.

Bra¨uer G, Ruske M, Szczyrbowski J Teschner G, Zmelty A (1998) Mid frequency sputtering with TwinMag< sup>®-a survey of recent results, 51:655-659.

Caglar, Y, Ilican S, Caglar M (2007). Single-oscillator model and determination of optical constants of spray pyrolyzed amorphous SnO2 thin films. Eur. Phys. J. B 58-251-256.

Dislich H, Hinz P (1982). History and principles of the sol-gel process, and some new multicomponent oxide coatings. J. Non-Cryst. Solids 48:11-16.

Doeuff S, Henry M, Sanchez C, Symp MRS (1986). The Gel Route to Tio_2Photoanodes. 73:653.

Dumitriu D, Bally AR, Ballif C, Hones P, Schmid PE, Sanjinés R, Lévy F, Pârvulescu VI (2000). Photocatalytic degradation of phenol by TiO2 thin films prepared by sputtering, Appl. Catal. B. Environ. 25:83-92.

El-Nahass M (1992). Optical properties of tin diselenide films. J. Mater. Sci. 27:6597-6604.

El-Nahass M, Atta A, El-Sayed H, El-Zaidia E (2008). Structural and optical properties of thermal evaporated magnesium phthalocyanine (MgPc) thin films. Appl. Surf. Sci. 254:2458-2465.

El-Nahass M, El-Barry A, El-Shazly E, Omar H (2010). Structural and optical properties of thermally evaporated cadmium thiogallate CdGa2S4 nanostructure films. Eur. Phys. J. Appl. Phys. 52:10502..

El-Nahass M, Soliman H, Hendi D, Mady KA (1992). Effect of some growth parameters on vacuum-deposited CuInSe2 films. J. Mater. Sci. 27:1484-1490.

El-Raheem MA, Amry A, Al-Mokhtar M, Al-Jalali M, Amin S, El-Sayed H, Al-Ofi H (2012). Transport properties of Aluminum-Doped Zinc Oxide Thin Films. Adv. Mater. Corros. 1:30-35.

Ghanashyam Krishna M, Pillier JS, Bhattacharya AK (1999). Variable optical absorption edge in ion beam sputtered thin ytterbium oxide films. Thin Solid Films- 357:218-222.

Henry BM (1978). US Patent 4, 200.

Hou YO, Zhuang DM, Zhang G, Zhao M, Wu MS (2003). Influence of annealing temperature on the properties of titanium oxide thin film. Appl. Surface Sci. 218:98-106.

Livage J (1986). Synthesis, structure and applications of TiO2 gels, Cambridge Univ. Press, 73:717-724.

Lo¨ bl P, Huppertz M, Mergel D (1994). Nucleation and growth in TiO2 films prepared by sputtering and evaporation. Thin Solid Films 251:72-79.

Lottiaux M, Boulesteix C, Nihoul G, Varnier F, Flory F, Galindo R, Pelletier E (1989). Morphology and structure of TiO2 thin layersvs. thickness and substrate temperature. Thin Solid Films, 170:107-126.

Macleon HA (1986). Thin Film Optical Filters, 2^{ed} ed., Adam Hilger Ltd., Bristol, P. 71.

Nabavi N, Doeuff S, Sanchez C Livage J (1989). Sol-gel synthesis of electrochromic films. Mater. Sci. Eng. B. 3:203-207.

Ozer N, Tepehan F, Bozkurt N (1992). An "all-gel" electrochromic

device. Thin Solid Films 219:193-198.
Pal U, Samanta D, Ghori S, Chaudhuri AK (1993). Optical constants of vacuum-evaporated polycrystalline cadmium selenide thin films. J. Appl. Phys. 74(10):6368-6374.
Pulker HK (1984). Coatings on Glass. Elsevier Science Publishers B. V. P. 311.
Ritter E (1975). Dielectric film materials for optical applications. Phys. Thin Films 8:1.
Robert M Jr., Morel DL, Ferekides CS (2005). Transparent conducting oxide thin films of Cd2SnO4 prepared by RF magnetron co-sputtering of the constituent binary oxides. Thin Solid Films 484:26-33.
Solomon I, Schmidt MP, Senemaud C, Khodja MD (1988). Band structure of carbonated amorphous silicon studied by optical, photoelectron, and x-ray spectroscopy. Phys. Rev. B 38:13263.
Takeda S, Suzuki S, Odaka H, Hosono H (2001). Photocatalytic TiO2 thin film deposited onto glass by DC magnetron sputtering. Thin Solid Films 392:338-344.
Takeda, S, Suzuki S, Odaka H (2001). Photocatalytic TiO2 thin film deposited onto glass by DC magnetron sputtering. Thin Solid Films. 392(2):338-344.
Timoumi A, Bouzouita H, Rezig B (2011). Optical constants of Na-In2S3 thin films prepared by vacuum thermal evaporation technique. Thin Solid Films 519:7615-7619.
Treichel O Kirchhoff V (2000). The influence of pulsed magnetron sputtering on topography and crystallinity of TiO2 films on glass. Surf. Coat. Technol. 123:268-272.
Urbach F (1953). The long-wavelength edge of photographic sensitivity and of the electronic absorption of solids. Phys. Rev. 92:1324.
WatanabeT, Fukayama S, Miyauchi M, Fujishima A, Hashimoto K (2000). Photocatalytic activity and photo-induced wettability conversion of TiO2 thin film prepared by sol-gel process on a soda-lime glass. J. Sol–Gel Sci. Technol. 19:71-76.
Wemple SH (1973). Refractive-index behavior of amorphous semiconductors and glasses. Rev. B. 7:3767.
Wemple SH, Didomenico Jr M (1971). Behavior of the electronic dielectric constant in covalent and ionic materials. Phys. Rev. B. 3:1338.
Yakuphanoglu F, Cukurovali A, Yilmaz I (2004). Determination and analysis of the dispersive optical constants of some organic thin films. Phys.B: Condensed Matt. 351:53-58.
Ya-Qi H, Da-Ming Z, Gong Z, Ming Z, Min-Sheng W (2003). Influence of annealing temperature on the properties of titanium oxide thin film. Appl. Surf. Sci. 218:97.
Yeung KS Lam YW (1983). A simple chemical vapour deposition method for depositing thin TiO2 films. Thin Solid ilms, pp. 109:169-178.
Yoko T, Kamiya K, Yuasa A, Tanaka K, Sakka S (1988). Surface modification of a TiO2 film electrode prepared by the sol-gel method and its effect on photoelectrochemical behavior. J. Non-Cryst. Solids 100:483-489.
Yoldas BE (1980). Investigations of porous oxides as an antireflective coating for glass surfaces. Appl. Opt. 19:1425-1429.
Yun, H, Miyazawa K, Honma I, Zhou H, Kuwabara M (2003). Synthesis of semicrystallizedmesoporous TiO2 thin films using triblock copolymer templates. Mater. Sci. Eng. C. 23:487-494.
Zhang F, Huang, N, Yang P, Zeng X, Mao Y, Zheng Z, Zhou Z, Liu X (1996). Blood compatibility of titanium oxide prepared by ion-beam-enhanced deposition. Surf. Coat. Technol. 84:476-479.

academicJournals

Vol. 8(31), pp. 1581-1587, 23 August, 2013
DOI: 10.5897/IJPS2013.3962
ISSN 1992 - 1950 © 2013 Academic Journals
http://www.academicjournals.org/IJPS

International Journal of Physical Sciences

Full Length Research Paper

Structural and DC Ionic conductivity studies of carboxy methylcellulose doped with ammonium nitrate as solid polymer electrolytes

K. H. Kamarudin and M. I. N. Isa*

Advanced Materials Research Group, Renewable Energy Research Interest Group, Department of Physical Sciences, Faculty of Science and Technology, Universiti Malaysia Terengganu, 21030 Kuala Terengganu, Terengganu, Malaysia.

Accepted 15 August, 2013

Solid polymer electrolytes have been prepared by solution casting technique. Carboxy methylcellulose (CMC)-ammonium nitrate (AN) films were studied with varied AN salt concentration from 5-50 wt.% at ambient temperature. X-ray diffraction (XRD) pattern shows the amorphous nature of polymer electrolyte samples. IR-spectra confirm the polymer-salt complexes in the range of 1633 - 829 cm^{-1}. Impedance analysis reveals that polymer electrolyte film containing 45wt.% AN exhibits the highest ionic conductivity of (7.71 ± 0.04) $x10^{-3}$ Scm^{-1}, while pure CMC film gives the lowest ionic conductivity of (1.86 ± 0.03) $x10^{-8}$ Scm^{-1}. It was evident from this study that the increase of ionic conductivity depends on the AN salt concentration. The present polymer-salt system has potential application in electrochemical devices based on the results obtained.

Key words: Carboxy methylcellulose, ammonium nitrate, solid polymer electrolytes, ionic conductivity.

INTRODUCTION

Since the earliest breakthrough of polymer-salt complexes by Wright in 1975, there was a plethora of research focusing on the study and development of solvent free polymer electrolytes (PEs). Extensive research on PEs were driven by their advantages such as ease of preparation, light weight, leakage free, mechanically stable and flexibility for packaging design over gel/liquid counterparts (Ramesh et al., 2002; Quartarone et al., 1998). PEs have become promising materials for electrochemical device applications, namely, high energy density rechargeable batteries, fuel cells, supercapacitors, sensors and electrochromic displays (Bhargav et al., 2009; Ma et al., 2013). Poor ionic conductivity as a result of the low segmental mobility of the polymer chain at ambient temperature is the major drawback possessed by solid Pes (Armand, 1994; Tarascon and Armand, 2001). To overcome the challenge, several approaches have been employed to enhance the room temperature conductivity as well as to improve the mechanical stability and interfacial activity of PEs including using chitin/chitosan, starch and cellulose derivates as organic/biodegradable polymer matrix incorporating with inorganic salts such as sodium salt and ammonium salt (Kumar et al., 2011; Hassan et al., 2010). Typically, ionic conduction in PEs are governed by the degree of crystallinity (Kumar et al., 2011), salt/acid concentration (Sit et al., 2012; Idris et al., 2009) as well as the nature of polymer and salt/acid.

Carboxy methylcellulose (CMC) is a natural anionic polysaccharide which is widely used in many industrial sectors including food, textiles, paper, adhesives, paints, pharmaceutics, cosmetics and mineral processing. CMC

*Corresponding author. E-mail: ikmar_isa@umt.edu.my. Tel: +609-6683111. Fax: +609-6694660.

Figure 1. The highly translucent and flexible CMC-AN solid polymer electrolyte films.

is a cellulose derivative prepared through etherification of the hydroxyl groups with sodium monochloroacetate in the presence of aqueous alkali (Pushpamalar et al., 2006). It is a natural organic polymer that is non-toxic, renewable, available in abundance, biocompatible and biodegradable (Adinugraha et al., 2005). Due to its highly hydrophilic properties, CMC can easily dissolve in cold/hot water.

Inorganic AN salt is widely utilized in the manufacture of nitrogen-rich inorganic fertilizers, as a major component in explosive mixtures (AN-fuel oil for mining) and in gas generator propellant formulations as well as rocket propellant oxidizer (Lang and Vyazovkin, 2008). AN exhibits five polymorphic crystal phases at atmospheric pressure from cryogenic temperatures up to its melting temperature of 442 K. The IV-phase shows an orthorhombic crystal structure at room temperature (Chellappa et al., 2012).

In this paper, we report the effect of ammonium salt concentration on the structural and ionic conductivity of CMC-AN polymer electrolytes at ambient temperature in preparation of solid-state rechargeable proton battery.

EXPERIMENTAL PROCEDURE

Polymer electrolytes

The sodium salt of CMC was obtained from Acros Organics (purity >99.9%; average MW = 90,000 and DS = 0.7). AN was purchased from Sigma Aldrich (purity 99%) and both materials were directly used without further treatment. Solution casting method was employed to obtain film samples with varied amount of ammonium salt concentration (5 – 50 wt.%). Pure CMC film without ammonium salt was also prepared as a control. In a clean beaker, weighted amounts of CMC powder and AN crystals were dissolved in 100 ml distilled water at room temperature. Complete dissolution was achieved after several hours stirring at room temperature using magnetic stirrer. The final clear solution was then poured into separate Petri dishes and left to dry at room temperature to form highly translucent and flexible thin films. Polymer electrolyte films were transferred to a dessicator for further drying prior to sample characterization.

Characterization techniques

In this work, X-ray diffraction (XRD) analysis was carried out using a MiniFlex II Rigaku with CuK_α radiation (λ = 1.5418 Å) at room temperature. The XRD patterns were recorded at Bragg angle (2θ) in the range of 10 - 60° with a scan speed of 2°/min. This technique was employed to determine the crystallinity of polymer electrolyte films.

The occurance of complexation and the presence of functional groups of polymer electrolyte films were analyzed using IR technique. The Fourier Transform InfraRed (FTIR) spectra were recorded using Thermo Nicolet 380 FTIR spectrometer equipped with an attenuated total reflection (ATR) accessory with a germanium crystal. The sample was pressed on a germanium crystal and infrared light was passed through the sample with the frequency ranging from 700 - 4000 cm^{-1} at spectra resolution of 4 cm^{-1}. The FTIR data was recorded in the transmittance mode.

Impedance spectroscopy measurements were performed to determine the ionic conductivity of polymer electrolyte films over a wide range of frequency. The measurements were carried out with an electrical impedance spectroscopy (EIS) HIOKI 3532–50 LCR Hi Tester interfaced to a personal computer in 50 – 1M Hz frequency range. A π cm^2 round piece of electrolyte film was pressed between two steel electrodes of sample holder in a temperature controlled MEMMERT oven.

RESULTS AND DISCUSSION

XRD analysis

Figure 1 shows a highly translucent and flexible thin film of CMC-AN solid polymer electrolytes obtained from solution casting technique. Typical XRD patterns obtained from CMC-AN polymer electrolyte films with varied AN concentrations are shown in Figure 2i. Figure 2ii and iii represent XRD patterns of pure AN crystals and

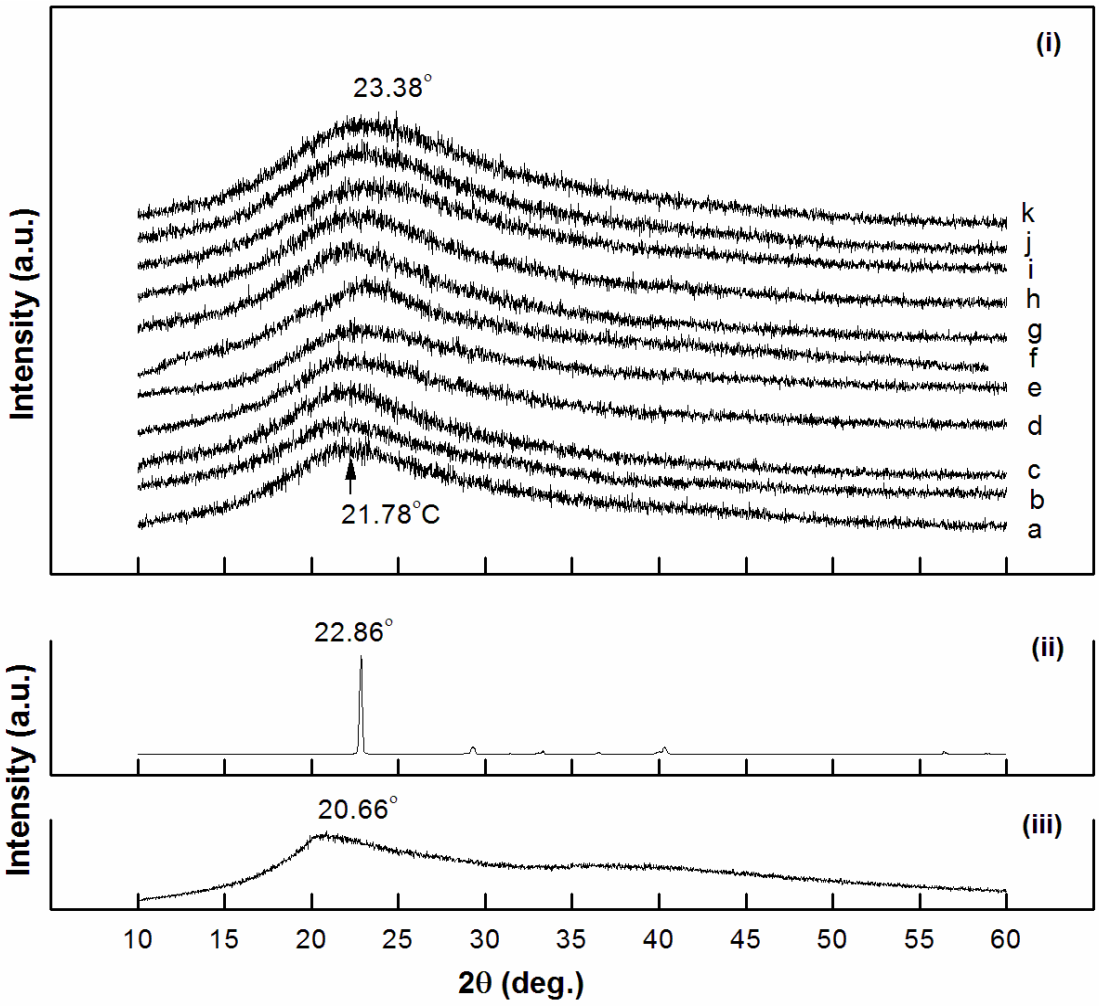

Figure 2. The XRD pattern of (i): Thin film samples containing CMC with varied amount of AN salt concentration, (a) Pure CMC, (b) CMC-5wt.% AN, (c) CMC-10wt.% AN,(d) CMC-15wt.% AN,(e) CMC-20wt.% AN,(f) CMC-25wt.% AN,(g) CMC-30wt.% AN,(h) CMC-35wt.% AN,(i) CMC-40wt.% AN,(j) CMC-45wt.% AN 5 and (k) CMC-50wt.% AN, (ii): Pure AN salt crystals, and (iii): Pure CMC powder.

CMC powder as references.

The XRD pattern for pure CMC powder (Figure 2iii) display a broad diffused hump centered at 2θ = 20.66°C and a small shoulder between 35°C and 45°C corresponding to the amorphous nature of pure CMC. The pattern for pure AN crystals show four polycrystalline peaks with the strongest intensity peak located at 2θ = 22.86°C (Figure 2ii). Upon addition of AN salt, the broad peaks tend to broaden and shift to a higher Bragg angle from 2θ = 21.78°C (pure CMC film) to 23.38°C (CMC-50wt.% AN) as can be seen in Figure 2i. The increase in broadness implies the amorphous nature of polymer electrolyte films with some localized ordering of the complex system (Selvasekarapandian et al., 2010). No additional peaks have been observed in the complex system indicating a complete dissociation of AN salt in the CMC polymer matrix. XRD patterns confirmed the amorphous nature of all polymer electrolyte films (Baril et al., 1997).

FTIR analysis

The occurance of complexation and the presence of functional groups in polymer electrolyte films were confirmed using IR Spectrophotometer. Different vibration modes of various functional groups of CMC and AN correspond to the observed IR characteristic peaks of polymer-salt system.

CMC and AN backbones

Pure CMC exhibits absorption band in the range of

Table 1. FTIR vibration modes of CMC and AN.

Band Assignment	CMC Wavenumber (cm^{-1})	AN Wavenumber (cm^{-1})
Bending mode of ether(glycosidic) linkage, δ(C-O-C)	1040, 1110	-
Bending mode of C-H band, δ(CH)	1377	-
Stretching mode of O-H in plane	1410	-
Stretching mode in carboxylic group, υ(C=O)	1605	-
Stretching mode of C-H band, υ(CH)	2920	-
Intra-molecular hydrogen bond, υ(OH)	3439	-
Symmetric bending band, $\delta(NO_3^-)$	-	828
Symmetric stretching mode, $\upsilon(NO_3^-)$	-	1043
Asymmetric stretching mode, $\upsilon(NO_3^-)$	-	1363
Stretching mode of N-H band, υ(NH)	-	3031
Intra-molecular hydrogen bond, υ(OH)	-	3251

1072 - 3439 cm^{-1} (Lii et al., 2002; Jiang et al., 2009). The main backbones in CMC observed at 1605 cm^{-1} and 1377 cm^{-1} correspond to C=O band and C-H bonding, respectively. In the case of AN, vibration bands have been found in the range of 828 - 3251cm^{-1} (Kadir et al., 2011; Majid and Arof, 2005). Typically, the O-H bonding can be found in the range of 3000 - 3800 cm^{-1} for both backbones. The vibration modes of CMC and AN are summarized in Table 1.

CMC-AN complexes

The occurrence of complexation between the polymer host and salt has been correlated to the spectral changes including shift of band, emergence of new bands or/and disappearance of bands. The complexation between CMC and inorganic salts/acids was reported to occur in the band range of 1600 - 1040 cm^{-1} (Chai and Isa, 2013; Samsudin and Isa, 2012). Therefore, detailed observation on the frequency region of 1800 - 800 cm^{-1} is required in this study. Outside of this region, insignificant or very weak peaks have been discovered.

Figure 3 depicts that adding a range of AN concentrations to CMC polymer electrolyte films resulted in the emergence of complexation bands in the range of 1633 - 829 cm^{-1}. The COO^- stretching band of CMC shifts to the lower wavenumber from 1591 - 1583 cm^{-1} and a new peak emerges at 1633 cm^{-1} as the AN concentration increases to 50wt.%. The new peak is associated to the H^+ ion originating from AN. Strong absorption peaks at 1417 and 1321 cm^{-1} assigned to O-H stretching in plane and symmetrical stretching of C-H bands of CMC respectively have shifted to 1431 and 1331 cm^{-1}. The shifting proved the complexation of CMC with the nitrate ions of AN. Similar behavior has been detected in the

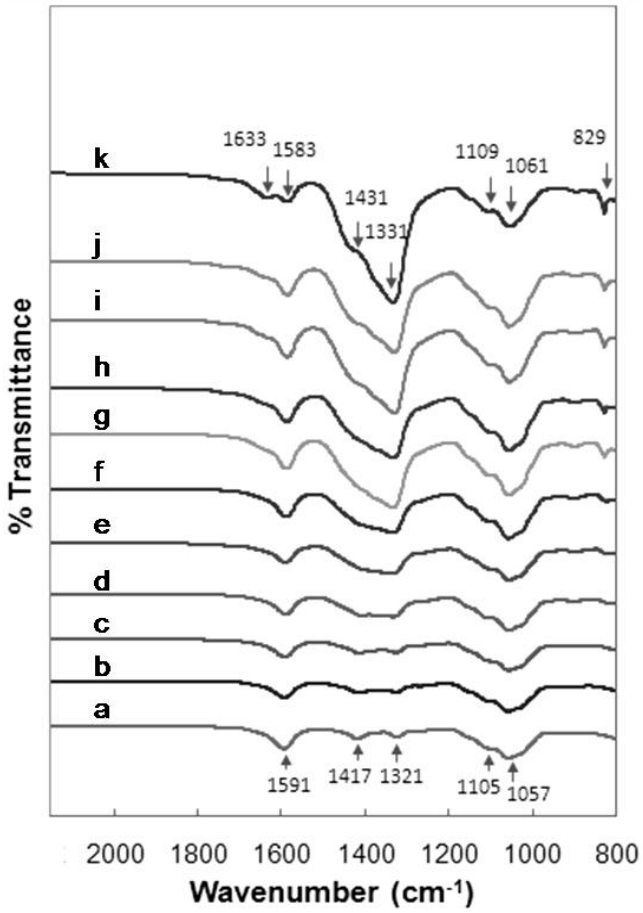

Figure 3. FTIR spectra of polymer electrolyte films containing CMC with varied amount of AN salt concentration, (a) Pure CMC film, (b) CMC-5wt.% AN, (c) CMC-10wt.% AN, (d) CMC-15wt.% AN, (e) CMC-20wt.% AN, (f) CMC-25wt.% AN, (g) CMC-30wt.% AN, (h) CMC-35wt.% AN, (i) CMC-40wt.% AN, (j) CMC-45wt.% AN 5 and (k) CMC-50wt.% AN.

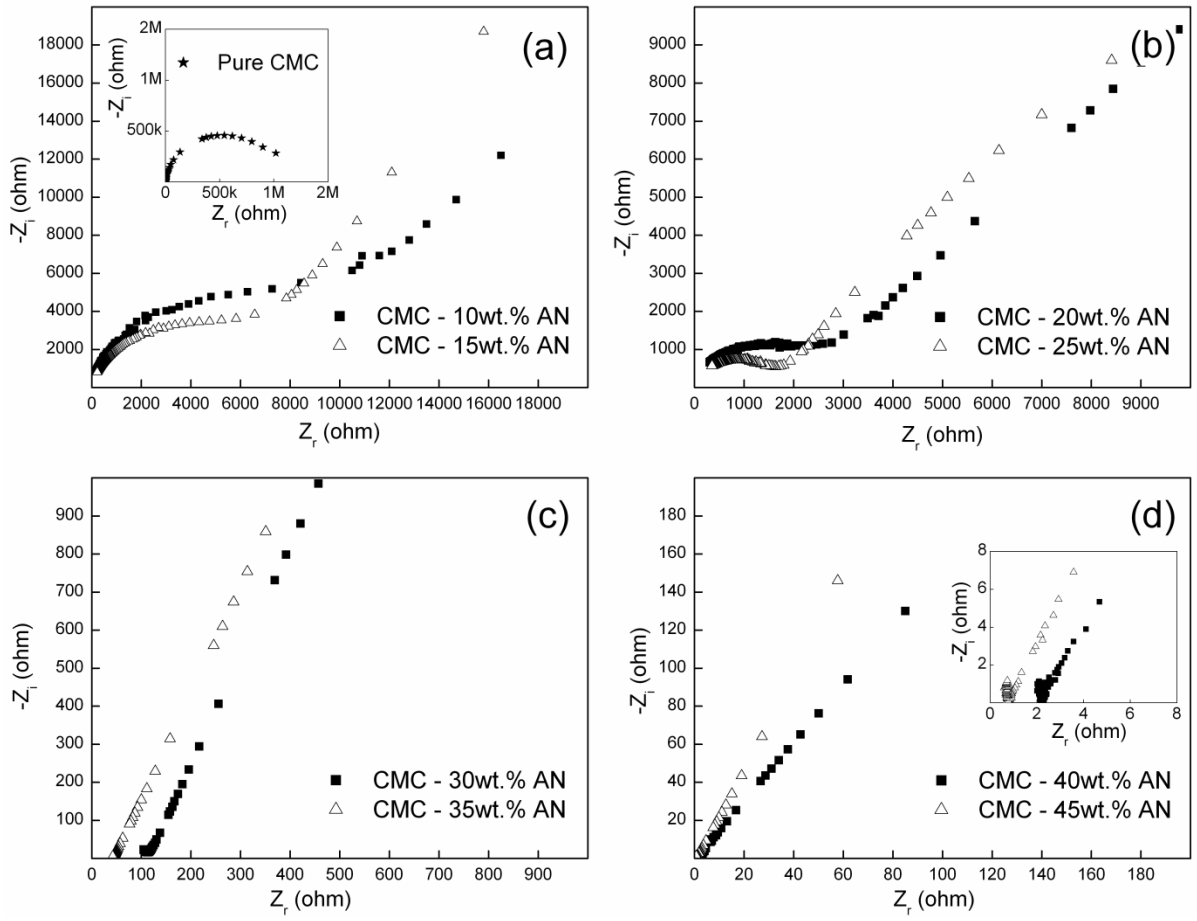

Figure 4. The Cole-Cole (Nyquist) plots of the real impedance, Z_r versus imaginary impedance, $-Z_i$ polymer electrolytes with varied amount of AN concentration at ambient temperature; (a) CMC-10wt.% AN and CMC-15wt.% AN (Inset: Pure CMC film), (b) CMC-20wt.% AN and CMC-25wt.% AN, (c) CMC-30wt.% AN and CMC-35wt.% AN, and (d) CMC-40wt.% AN and CMC-45wt.% AN (Inset: Enlargement of (d)).

region of 1105 - 1057 cm^{-1} which signifies the characteristic of polysaccharide skeleton. No obvious changes of intensity have been observed except shifting of the bands to the higher wavenumbers. A new peak at 829 cm^{-1} corresponds to the nitrate ion of AN. It can be concluded from the analysis that the protonation has occurred in the present polymer-salt complexes and the interactions between CMC and AN has been established.

Impedance analysis

Cole-cole plots

Figure 4 shows the complex impedance plots of pure CMC film and CMC-AN doped with different concentration of AN at ambient temperature. The figure shows a part of a depressed semicircle for pure CMC film. The high frequency semicircle is associated to the parallel combination of the bulk resistance and bulk capacitance as a result of protons migration and immobile polymer chains, respectively (Selvasekarapandian et al., 2010; Subban et al., 2005). As the salt concentration begins to increase, the semicircle in the plots become to lessen. The depressed semicircle and inclined spikes (Figure 4a-b) implies that the ions have different relaxation times (Subban et al., 2005). Beyond 25wt.% AN, the appearance of low frequency spikes indicate that only the resistive component of the polymer electrolyte predominate (Selvasekarapandian et al., 2010) as illustrated in Figure 4c-d. The bulk resistance, R_b can be calculated from the intercept of high frequency semicircle or the low frequency spike on the Z_r-axis.

dc ionic conductivity

The high ionic conductivity of solid polymer electrolytes is mainly governed by two important factors; that is, ionic

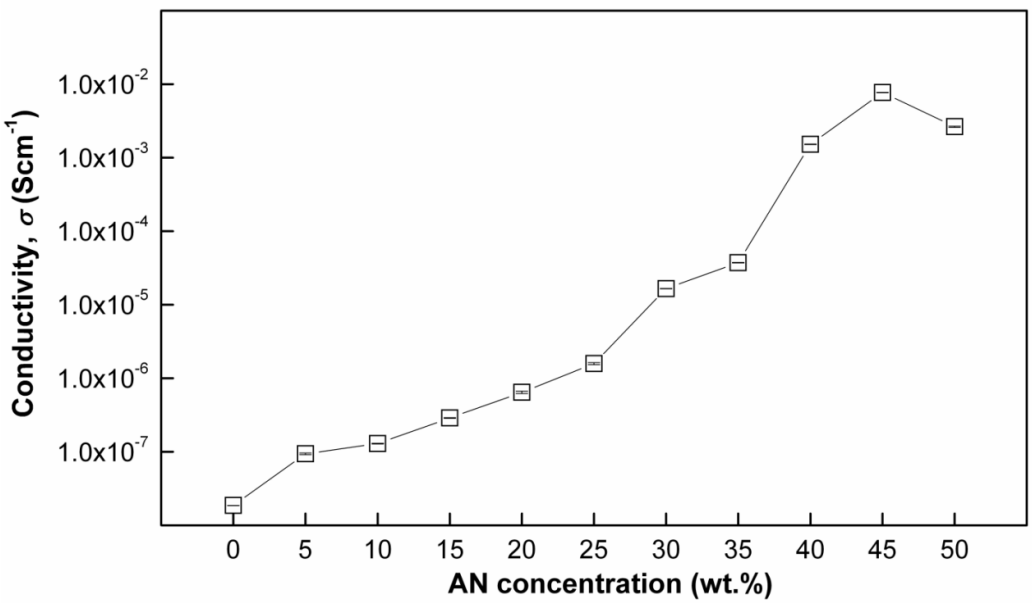

Figure 5. Graph of ionic conductivity, σ versus AN salt concentration of polymer electrolyte films at ambient temperature, 303K.

conducting species concentration, η and the charge carrier mobility, μ along with the type of charge carriers (cationic/anionic) and temperature (Hirankumar et al., 2005; Raphael et al., 2010). The evolution of the ambient temperature, 30°C (303K) ionic conductivity of polymer electrolyte films as a function of the AN concentration is shown in Figure 5. The ionic conductivity of polymer electrolyte films, σ were calculated using Equation 1:

$$\sigma = \frac{t}{R_b A} \quad (1)$$

To attain the ionic conductivity, σ (Scm^{-1}), the thickness of the electrolyte, t (cm), the bulk resistance, R_b (Ω), and the area of electrolyte-electrodes contact, A (cm^2) should be known. Concentration dependence of ionic conductivity provides information on the specific interaction between the salt and polymer matrix.

As illustrated in Figure 5, the ionic conductivity increases gradually with the addition of AN concentration up to 45wt.%. The increment of ionic conductivity with increasing AN concentration can be related to the increasing number of mobile charge carriers and/or their mobility (Samsudin and Isa, 2012). This may also be attributed to an increase of the amorphous nature of polymer electrolytes as confirmed by the XRD analysis. The optimum AN concentration of 45 wt.% gives the highest ionic conductivity of (7.71 ± 0.04) $x10^{-3}$ Scm^{-1} compared to pure CMC film of (1.86 ± 0.03) $x10^{-8}$ Scm^{-1}. Beyond that, the ionic conductivity decreases. The subsequent decrease at AN concentration of 50 wt.% could be caused by the formation of ion multiples or ion aggregates which reduces the number of mobile ions and limits its mobility in the polymer electrolytes (Woo et al., 2011; Yahya and Arof, 2003). At such high concentration, polymer electrolyte film was observed mechanically unstable. This was evidenced by the reduction in film flexibility as a consequence of rapid increase in viscosity (Ferry et al., 1998). Table 2 summarizes the ionic conductivity of single polymer-ammonium salt system at room temperature as reported in the literatures. The list indicates that the ionic conductivity obtained from the present work is higher compared to the previous works reported for similar AN salt system.

Conclusion

The new solid polymer electrolytes based on CMC and AN have been successfully prepared by solution cast method. XRD studies confirmed that all films were predominantly amorphous. IR spectra indicated that the complexation of polymer electrolyte films occured in the frequency range of 1633 - 829 cm^{-1}. The study revealed that the concentration of AN greatly influenced the ionic conductivity of the polymer electrolyte films. The pure CMC film gives the ionic conductivity in the order of 10^{-8} Scm^{-1}. Upon addition of the salt, the ionic conductivity has increased to the optimum AN concentration (45 wt.%) in the order of 10^{-3} Scm^{-1} at ambient temperature. The present polymer electrolytes were identified as promising materials for electrochemical device applications.

Table 2. Ionic conductivity of solid polymer electrolytes based on single polymer and AN salt system measured at room temperature from literatures compared to the present work.

Polymer host	AN concentration (wt.%)	Solvent	Conductivity, σ (Scm^{-1})	Reference
Chitosan	45	Distilled water	2.53×10^{-5}	Majid and Arof (2005)
Chitosan	40	Acetic acid	8.38×10^{-5}	Ng and Mohamad (2006)
Methylcellulose	25	Distilled water	2.10×10^{-6}	Shuhaimi et al. (2010)
Tapioca starch	25	Oxalic acid	2.15×10^{-6}	Azlan and Isa (2011)
Tapioca starch	25	Distilled water	2.83×10^{-5}	Khiar and Arof (2010)
CMC	45	Distilled water	$(7.71 \pm 0.04) \times 10^{-3}$	Present work

ACKNOWLEDGEMENT

The authors would like to acknowledge laboratory assistants of Department of Physical Sciences, Universiti Malaysia Terengganu for the assistance during sample preparation and characterization. The authors also grateful to Universiti Malaysia Terengganu for financial support through *Geran Galakan Penyelidikan (GGP) 68007/2013/58*.

REFERENCES

Adinugraha MP, Marseno DW, Haryadi (2005). Synthesis and characterization of sodium carboxymethylcellulose from cavendish banana pseudo stem (*Musa cavendishii* LAMBERT). Carbohydr. Polym. 62:164-169.

Armand M (1994). The history of polymer electrolytes. Solid State Ionics. 69:309-319.

Azlan AL, Isa MIN (2011). Proton conducting biopolymer electrolytes based on tapioca starch- NH_4NO_3. Solid State Sci. Technol. Lett. 18:124-129.

Baril D, Michot C, Armand M (1997). Eletrochemistry ofliquid vs. Solid: Polymer electrolytes. Solid State Ionics 94:35-47.

Bhargav PB, Mohan VM, Sharma AK, Rao VVRN (2009). Investigations on electrical properties of (PVA:NaF) polymer electrolytes for electrochemical cell applications. Curr. Appl. Phys. 9:165-171.

Chai MN, Isa MIN (2013). The oleic acid composition effect on the carboxymethyl cellulose based biopolymer electrolyte. J. Crystallization Process Technol. 3:1-4.

Chellappa RS, Dattelbaum DM, Velisavljevic N, Sheffield S (2012). The phase diagram of ammonium nitrate. J. Chem. Phys. 137:064504.

Ferry A, Oradd G, Jacobsson P (1998). Ionic interactions and transport in a low-molecular-weight model polymer electrolyte. J. Chem. Phys. 108:7426-7433.

Hassan MA, Gouda ME, Sheha E (2010). Investigations on the electrical and structural properties of PVA doped with $(NH_4)_2SO_4$. J. Appl. Polym. Sci. 116:1213-1217.

Idris NK, Aziz NAN, Zambri MSM, Zakaria NA, Isa MIN (2009). Ionic conductivity studies of chitosan-based polymer electrolytes doped with adipic acid. Ionics. 15:643-646.

Jiang LY, Li YB, Zhang L, Wang XJ (2009). Preparation and characterization of a novel composite containing carboxymethyl cellulose used for bone repair. Mater. Sci. Eng. C. 29:193-198.

Kadir MFZ, Aspanut Z, Majid SR, Arof AK (2011). Ftir studies of plasticized poly(vinyl alcohol)–chitosan blend doped with NH_4NO_3polymer electrolyte membrane. Spectrochim. Acta, Part A. 78:1068-1074.

Khiar ASA, Arof AK (2010). Conductivity studies of starch-based polymer electrolytes. Ionics 16:123-129.

Kumar KK, Ravi M, Pavani Y, Bhavani S, Sharma AK, Rao VVRN (2011). Investigations on the effect of complexation of NaF salt with polymer blend (PEO/PVP) electrolytes on ionic conductivity and optical energy band gaps. Physica B. 406:1706-1712.

Lang AJ, Vyazovkin S (2008). Phase and thermal stabilization of ammonium nitrate in the form of PVP–AN glass. Mater. Lett. 62:1757-1760.

Lii C-Y, Tomasik P, Zaleska H, Liaw S-C, Lai VMF (2002). Carboxymethyl cellulose–gelatin complexes. Carbohydr. Polym. 50:19-26.

Ma J, Sahai Y (2013). Chitosan biopolymer for fuel cell applications. Carbohydr. Polym. 92:955-975.

Majid SR, Arof AK (2005). Proton-conducting polymer electrolyte films based on chitosan acetate complexed with NH_4NO_3 salt. Phys. B. 355:78-82.

Ng LS, Mohamad AA (2006). Protonic battery based on a plasticized chitosan-NH_4NO_3 solid polymer electrolyte. J. Power Sources 163:382-385.

Pushpamalar V, Langford SJ, Ahmad M, Lim YY (2006). Optimization of reaction conditions for preparing carboxymethyl cellulose from sago waste. Carbohydr. Polym. 64:12-18.

Quartarone E, Mustarelli P, Magistris A (1998). PEO-based composite polymer electrolytes. Solid State Ionics 110:1-14.

Ramesh S, Yahaya AH, Arof AK (2002). Dielectric behaviour of PVC-based polymer electrolytes. Solid State Ionics 152-153:291-294.

Samsudin AS, Isa MIN (2012). Structural and ionic transport study on CMC doped NH_4Br: A new types of biopolymer electrolytes. J. Appl. Sci. 12:174-179.

Selvasekarapandian S, Hema M, Kawamura J, Kamishima O, Baskaran R (2010). Characterization of PVA-NH_4NO_3 polymer electrolyte and its application in rechargeable proton battery. J. Phys. Soc. Jpn. 79SA:163-168.

Shuhaimi NEA, Teo LP, Majid SR, Arof AK (2010). Transport studies of NH_4NO_3 doped methyl cellulose electrolyte. Synth. Met. 160:1040-1044.

Sit YK, Samsudin AS, Isa MIN (2012). Ionic conductivity study on hydroxyethyl cellulose (HEC) doped with NH_4Br based biopolymer electrolytes. Res. J. Recent Sci. 1:16-21.

Subban RHY, Ahmad AH, Kamarulzaman N, Ali AMM (2005). Effects of plasticiser on the lithium ionic conductivity of polymer electrolyte PVC-$LiCF_3SO_3$. Ionics 11:442-445.

Tarascon JM, Armand M (2001). Issues and challenges facing rechargeable lithium batteries. Nature 414:359-367.

Woo HJ, Majid SR, Arof AK (2011). Conduction and thermal properties of a proton conducting polymer electrolyte based on poly (ε-caprolactone). Solid State Ionics 199-200:14-20.

Yahya MZA, Arof AK (2003). Effect of oleic acid plasticizer on chitosan–lithium acetate solid polymer electrolytes. Eur. Polym. J. 39:897-902.

academicJournals

Vol. 8(31), pp. 1588-1596, 23 August, 2013
DOI: 10.5897/IJPS10.539
ISSN 1992 - 1950 © 2013 Academic Journals
http://www.academicjournals.org/IJPS

International Journal of Physical Sciences

Full Length Research Paper

Flow behaviour of polyvinyl alcohol (PVOH) modified blends of polyvinyl acetate (PVAc)/natural rubber (NR) latexes

Stephen Shaibu Ochigbo

Department of Chemistry, Federal University of Technology, P. M. B. 65, Minna, Niger State, Nigeria.

Accepted 15 August, 2013

During compounding processes, polymer latexes are mixed with various colloidal systems (in particular, PVOH) or surface-active agents to modify the flow behaviour in order to suit the manufacturing process. In this study, the flow behaviour of aqueous dispersed PVAc, NR and different mixed dispersions were investigated both in the absence and presence of PVOH as flow modifier, using an Ostwald glass capillary viscometer. The results show an almost linear decrease in the relative viscosity of the NR/PVAc dispersion mixtures in the absence of a modifier, but the presence of different amounts of PVOH gave rise to significant deviations from this behaviour. It was found that these changes in the relative viscosities are governed by a balance between the following four effects: (i) the higher mobility of the NR chains compared to those of PVAc, which generally caused a decrease in the viscosities of the dispersion mixtures; (ii) the physical adsorption of PVOH on the NR chains that slowed down the movement of these chains and caused an increase in relative viscosity; (iii) the chemical interaction between the functional groups on PVAc and PVOH that gave rise to latex thickening and increased the relative viscosity; (iv) a dilution effect which reduced the viscosity, unless counterbalanced by one or more of the other effects.

Key words: Dispersion flow behaviour, viscosity, rubber latex, polyvinyl alcohol, polyvinyl acetate.

INTRODUCTION

Latexes are polymer particles dispersed in water. Their prominence has arisen because of mounting pressure from Environmental Protection Agencies (EPAs) against industrialists and researchers to replace solvent based systems with water based counterparts. Latex-based systems are all water based, without organic content, using only very small amounts of the latter to modify the final film properties, paint flow or rheological properties (Amalvy and Soria, 1996; Nabuurs et al., 1996; Meng et al., 2008). Because water is inexhaustible, cheap and readily available in comparison to organic solvents, latex based systems have corresponding advantages over their solvent based counterparts. In addition, the use of latex-based systems controls pollution, reduces risks of fire occurrence, and improves aspects of occupational health and safety (Zhaoying et al., 2001; Tambe et al., 2008; Kosto and Schall, 2007; Chen et al., 2005).

Polyvinyl acetate (PVAc) is an example of a synthetic polymer latex, for which the term “emulsion” is usually used in preference to latex, because it is a product of emulsion polymerization of the vinyl acetate monomer. PVAc emulsions have been used in large quantities in several application fields, especially in adhesives of papers and woods (Okaya et al., 1993; Backman and Lindberg, 2004; Kim and Kim, 2006). Because of its structural configuration, PVAc film is resistant to both oils

E-mail: stephen_ochigbo@yahoo.com. Tel: +234(0) 813 228 6172.

and ultra-violet (UV) radiation. However, the pendant acetate groups restrict free rotation along the C-C axis, thus resulting in a dry film which, besides having poor resistance to water, is too brittle and hence unsuitable in packaging applications unless in the presence of added plasticizer. On the other hand, natural rubber (NR) latex is a natural biosynthetic polymer which is derived from the tree *Hevea brasiliensis*. The latex that is obtained fresh from the tree (field latex) contains about 70% water, part of which should be removed to concentrate the latex for a wide variety of applications. The resulting latex concentrate has excellent physical properties and is used for the manufacture of dipped goods, adhesives/binders, thread, carpets/rugs, and moulded foams. Among these, the dipped goods, which include hand gloves, balloons, condoms, bladders, and catheters/tubes account for up to 60% NR latex usage (Haque et al., 1995; Sanguansap et al., 2005; Yip and Cacioli, 2002). However, the film cast from NR latex, unlike PVAc, is soft and tacky and possesses poor resistance to oil (Sirisinha et al., 2003), as well as poor resistance to both ultra violet (UV) radiation and ozone. Blending of polymer emulsions or dispersions is required in order to balance factors such as ease of application, wettability, drying characteristics, bond strength, clarity, environmental resistance, and especially cost (Meng et al., 2008). NR latex has intrinsic water resistance and toughness and therefore can improve water resistance behaviour of PVAc while the former simultaneously can improve in oil and ozone resistance when the latex and emulsion are blended together.

During the compounding processes, latexes are mixed with various colloid systems, in particular, poly (vinyl alcohol) (PVOH)) or surface-active agents to modify the flow behaviour in order to suit the manufacturing process (Schoeder and Brown, 1951; Brown and Garrett, 1959; Irving, 1990; Geurink et al., 1996; Hellgren et al., 1999. The flow behaviour of latexes is a critical factor, as it provides a guide for the formulation and ease of processing. A latex compound with a low viscosity and some thixotropic nature is good for dipping operations. The count of a latex thread is influenced by its viscosity (Peethambaran et al., 1990; Blackley, 1966; Calvert, 1982). Studies were carried out to examine the effect of PVOH on a PVAc emulsion (Dibbern-Brunelli and Atvars, 1995; Dibbern-Brunelli et al., 1998) and on NR latex (Peethambaran et al., 1990). An emulsion stabilized with PVOH has many advantages over surfactants, including Newtonian fluidity, superior primary wet tackiness, high strength and creep resistant film properties (Nakamae et al., 1999). This study used an Ostwald glass capillary viscometer to examine the flow behaviour of blends of PVAc/NR latexes in the presence of PVOH as a flow modifier. Owing to its simplicity, viscometry is popularly employed for studying compatibility as well as flow behaviour of polymers in solution (Singh and Singh, 1983; Kuleznev et al., 1978; Hourston and Hughes, 1978).

MATERIALS AND METHODS

A PVAc homopolymer emulsion was obtained from Makeean Polymers, South Africa with the trade name ML50 (solids contents = 52.5%, pH = 6.5). Field NR latex was provided by the Rubber Research Institute of Nigeria (RRIN), Iyanomo. It has a solid content of 45%. The PVOH was a Merck grade quality.

A dilute aqueous dispersion of the PVAc emulsion was prepared with a fixed concentration of 10 wt.%, designated PVAc_10. NR latex was prepared in different concentrations of 10 wt.% (NR_10), 5 wt.% (NR_5), and 1 wt.% (NR_1). All the dispersions were prepared relative to the respective dry solids contents of the original latexes. The prepared dispersions were in each case immediately passed through a stainless steel sieve with aperture 150 µm in order to remove any foreign suspended particles that may block the capillary of the Ostwald viscometer. An appropriate amount of PVOH was dissolved in water, under magnetic stirring at 90°C, to obtain a 2 wt.% stock solution from which lower concentrations of 1 wt.% and 0.5 wt.% were in turn prepared by successive dilution using de-ionised water. NR_10/PVAc_10, NR_5/PVAc_10, and NR_1/PVAc_10 were respectively blended into w/w compositions of 0/100, 25/75, 50/50, 75/25 and 100/0. This mixing method whereby the concentration of one component, PVAc (called the host polymer) is held constant while the concentration of the second, NR (called the guest polymer) is varied is known as the polymer-solvent method (Danait and Deshpande, 1995; Papanagopoulos and Dondos, 1996; Haiyang et al., 2000). In this paper, the method was applied to polymer dispersions rather than to conventional solution based polymer systems.

The flow rate (efflux time) of the different samples were directly observed as the time, t, needed for the liquid to pass through the capillary (Billmeyer, 1984). Measurements were made in the absence and presence of PVOH at a temperature of 22 ± 0.5°C. From the efflux times, the relative viscosities were calculated using Equation 1.

$$\eta_{rel} = t/t_o \quad (1)$$

Where, η_{rel} = relative viscosity, t = efflux time of dispersion, t_o = efflux time of pure water.

RESULTS AND DISCUSSION

The variation of relative viscosity with blend composition is represented by NR_10/ PVAc_10 blend, as shown in Figure 1. With increases in NR content, it is observed that the relative viscosity for the untreated sample (0 wt.% PVOH) decreases more rapidly than those for the samples containing different amounts of PVOH. This is attributed to the fact that NR latex is a pseudoplastic fluid, and even at rest the rubber particles are in random motion (Peethambaran et al., 1990). Therefore, as NR content increases, there results a corresponding increase in random motion and hence, an enhanced flow which leads to the observed marked decrease in viscosity of the untreated sample. On the other hand, the dispersions containing the different amounts (0.5, 1 and 2 wt.%) of PVOH show gradual and parallel decreases in viscosity with increasing NR content. It is suggested that the observed gradual and parallel decrease in viscosity of the PVOH-modified samples with increasing NR content, compared to that of the untreated sample, might be due

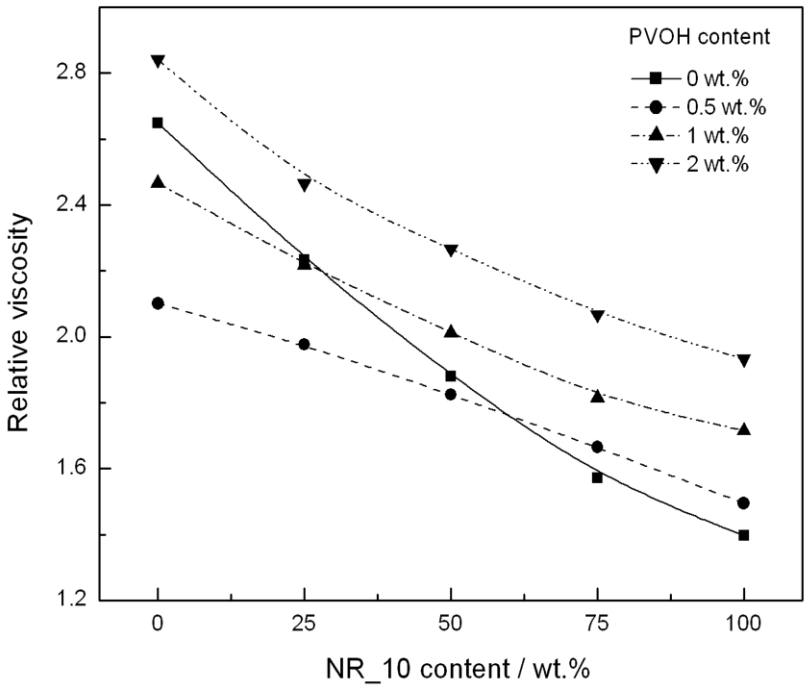

Figure 1. Dependence of relative viscosity on the blends' composition at various contents of PVOH modifier.

to adsorption of PVOH particles onto the NR particles. This adsorption could slow down the speed of the randomly moving NR particles and give rise to the observed trend of decrease in viscosity of the mixtures in the presence of PVOH. This agrees with the results of Peethambaran et al. (1990) in a study carried out to investigate the role of various surfactants on the viscosity of natural rubber latex.

Figure 2 presents the change in relative viscosity of the various unblended dispersions against different PVOH contents. The viscosity of pure PVAc (PVAc_10) is at maximum throughout the concentration range of the surfactant. Primarily, the viscosity of PVAc is intrinsically due to restricted mobility of the chains arising from steric hindrance between the acetate groups on one hand and then intermolecular dipole-dipole attraction between adjacent acetate functional groups. In addition, the high concentration of the PVAC_10 (that is, 10wt.%) which means that there are much chains condensed within a small volume, permitting intermolecular entanglements contributes to observed high viscosity. The viscosity of NR_10 of equivalent concentration (that is, 10 wt.%) by comparison is considerably lower than that of PVAc_10 as observed due to the fact that the particles of natural rubber is in constant random motion (pseudoplastic). Of course, NR_5 and NR_1 have lowered viscosity comparatively due to dilution effect and also pseudoplastic nature of the natural rubber latex as stated earlier.

The addition of the 0.5% PVOH immediately results in a significant drop in the relative viscosity curve for PVAc_10 observed. This concentration of PVOH is very dilute. So the accompanying relatively high water content imparts a plasticizing effect on the PVAc emulsion and thus causing its viscosity to drop sharply as observed. However, with higher concentration of PVOH, the viscosity values of PVAc_10 slightly improve after the depression. This improvement is as a result of the overshadowing of any plasticizing effect of the water content of the modifier by viscosity increase attributed firstly to adsorption of PVOH onto PVAc particles. An additional reason for the increase in viscosity is a consequence of the partial hydrolysis of the acetate functional group into carboxylate ions which in turns allows absorption (dissolution) of PVAc into PVOH (Lloyd, 1989; Hornby and Peach, 1993). These ions are capable of taking part in hydrogen bonded interactions with the hydroxyl groups of the modifier and, therefore, can contribute to the viscosity increase of the mixture. Interactions of this kind between particles of emulsion and aqueous polymeric solutions, leading to viscosity increases, have earlier been reported and the phenomenon is called latex thickening (Brown and Garrett, 1959). Several competitive interactions were postulated to account for the overall rheological behaviour of such mixtures. There were a number of observations providing evidence that the process involved in latex thickening is not merely that of the

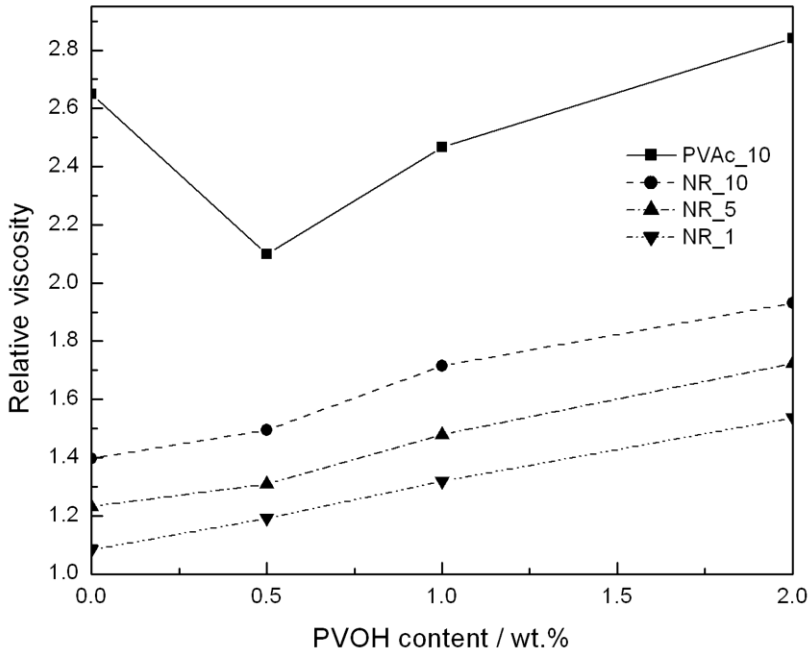

Figure 2. Dependence of relative viscosity on PVOH modifier content for various unblended aqueous dispersions.

enhancement of the viscosity of the continuous (water) phase by the water soluble polymer. There was also very little correlation between the aqueous viscosity of a polymer and its efficiency in thickening latexes. The significant drop in relative viscosity at 0.5% PVOH is attributed to the corresponding drop in concentration of the emulsion (PVAc_10) due to a dilution effect caused by the mixing of the two dispersions, which at this PVOH concentration dominated the latex thickening effect. The viscosity increase observed for the higher concentrated PVOH-modified samples is because of the latex thickening effect becoming more dominant.

The relative viscosities of the NR-based dispersions (with and without PVOH) are generally lower than that of the PVAc dispersion, which is due to the pseudoplasticity of NR, while the differences between the different NR dispersions are attributed to their corresponding differences in concentration. The relative viscosities of all the NR dispersions increase more or less linearly with increasing PVOH content. This behaviour shows that a completely different mechanism decides the interaction between NR and PVOH. As previously reported (Peethambaran et al., 1990), this involves a physical adsorption of PVOH solutes on the surfaces of the NR particles, which reduces the mobility of the NR particles.

The changes in the relative viscosities of the blended dispersions as a function of PVOH content are shown in Figures 3 - 5. These results clearly show the competition between the different influences discussed earlier. For all the blended dispersions, the viscosity generally increases with increasing PVOH content, but decreases according to the order: NR_10/ PVAc_10> NR_5/PVAc_10 >NR_1/PVAc_10. The increase with increasing PVOH content is the result of a combination of the latex thickening and physical adsorption effects discussed previously, while the decrease with increasing NR_10/5/1:PVAc_10 ratio is the result of the higher mobility of the NR chains. However, a dilution effect comes into play when more dilute NR dispersions are used, and therefore there is a decrease in relative viscosity with decreasing NR content in the NR dispersions that were mixed with the PVAc_10 dispersion at a constant ratio. This dilution effect also manifests itself in the lower than expected viscosities at 0.5% PVOH (as discussed above), but the physical adsorption between PVOH and NR becomes more dominant as the NR_10/5/1:PVAc_10 ratio increases in the dispersion mixtures, and the decrease in viscosity for the 0.5% PVOH containing samples disappears for the 75:25 NR_10/5/1:PVAc_10 dispersion mixture.

Utracki and Kanial (1982) divided viscosity-composition curves into three types on the basis of their deviation from the log-additivity rule ($\ln \eta_b = \Sigma \Phi_i \ln \eta_i$, in which η_b represents the blend viscosity, and Φ_i and η_i are the volume fraction and viscosity of component i in the blend). Based on this rule, Figures 6 - 9 were obtained, showing a comparison of the experimental and theoretical relative viscosities as a function of dispersion composition in the presence of different amounts of PVOH. As seen, all the experimental curves show

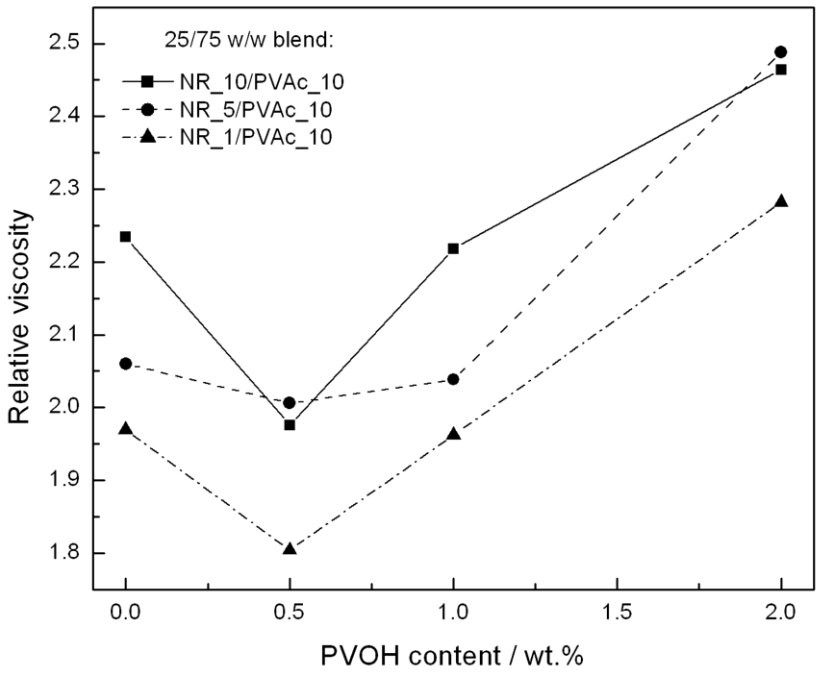

Figure 3. Dependence of relative viscosity on PVOH modifier content for different 25:75 w/w NR/PVAc blends.

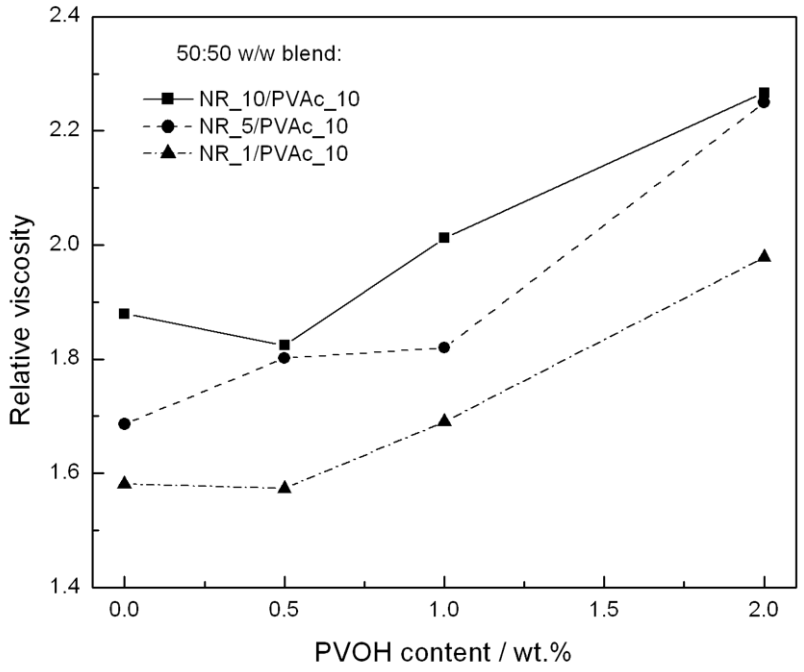

Figure 4. Dependence of relative viscosity on PVOH modifier content for different 50:50 w/w NR/PVAc blends.

deviations from the theoretical values. The linear (theoretical) curves indicate ideal behaviour which is exemplified by a situation in which particles of the mixed components consist of similar sizes in a given medium.

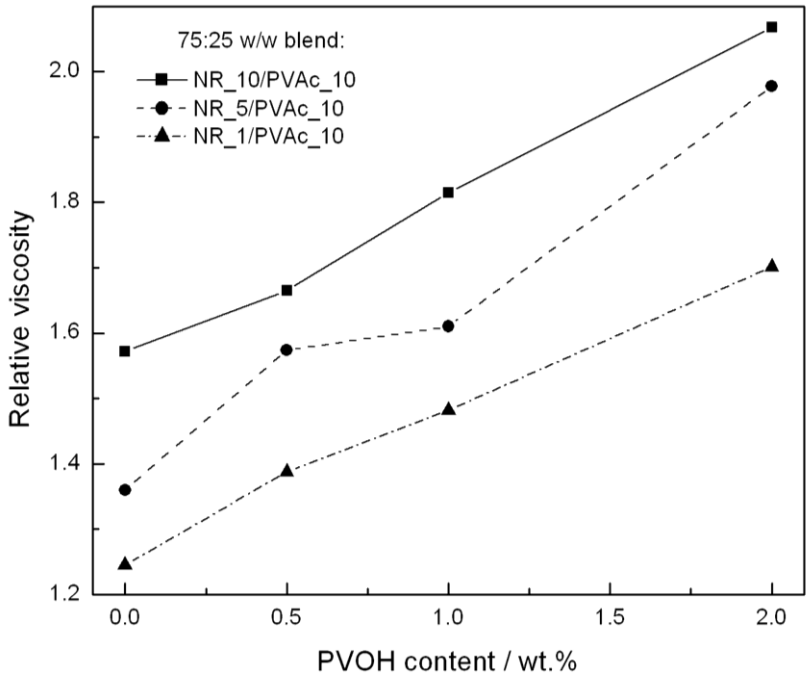

Figure 5. Dependence of relative viscosity on PVOH modifier content for 75:25 w/w NR/PVAc blends.

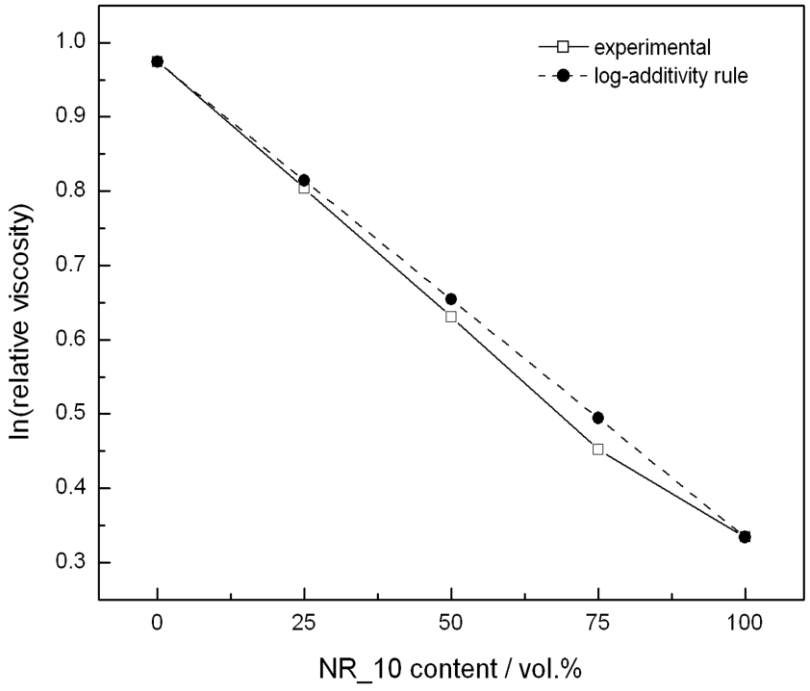

Figure 6. Comparison between experimental and theoretical viscosities for aqueous dispersions of NR_10/PVAc_10 without PVOH.

Such behaviour is in agreement with the additive rule (Wong, 1991). The observed deviations are evidence of interactions taking place between the mixed components, namely NR, PVAc, PVOH and water. Negative deviations

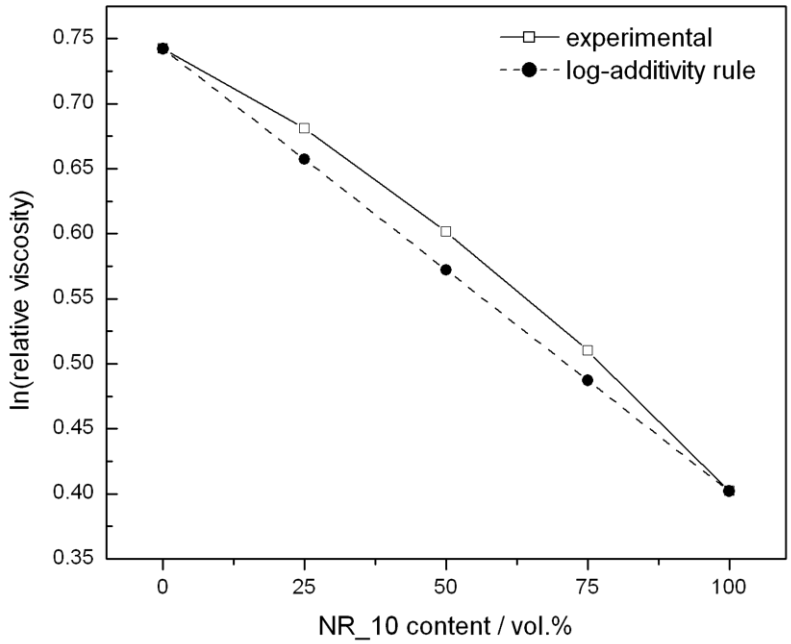

Figure 7. Comparison between experimental and theoretical viscosities for aqueous dispersions of NR_10/PVAc_10 with 0.5 wt.% PVOH.

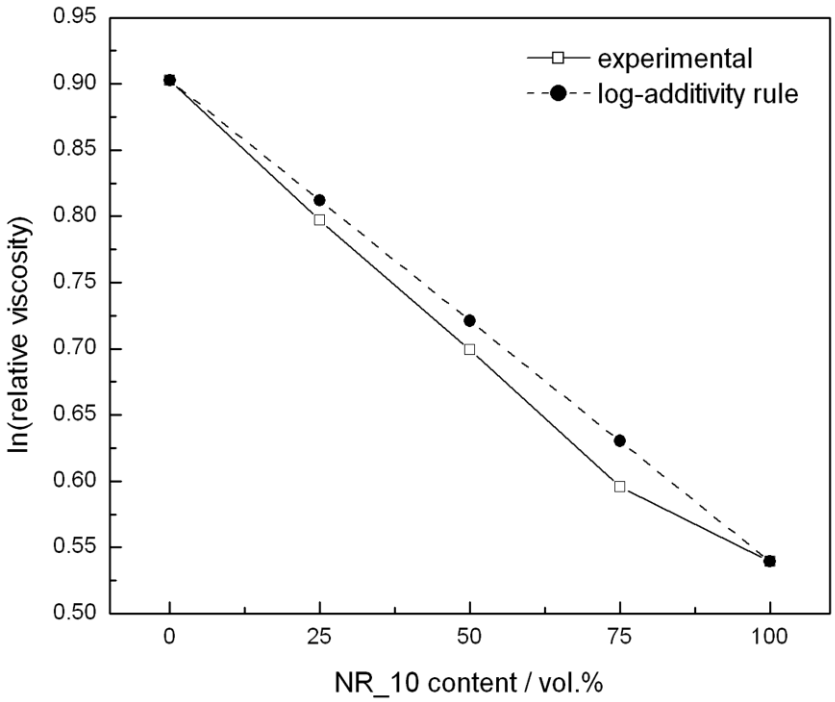

Figure 8. Comparison between experimental and theoretical viscosities for aqueous dispersions of NR_10/PVAc_10 with 1 wt.% PVOH.

are attributed to lowered mobility of particles, and hence reduced interactions between components, whereas positive deviations indicate that there are enhanced interactions between the components due to high mobility

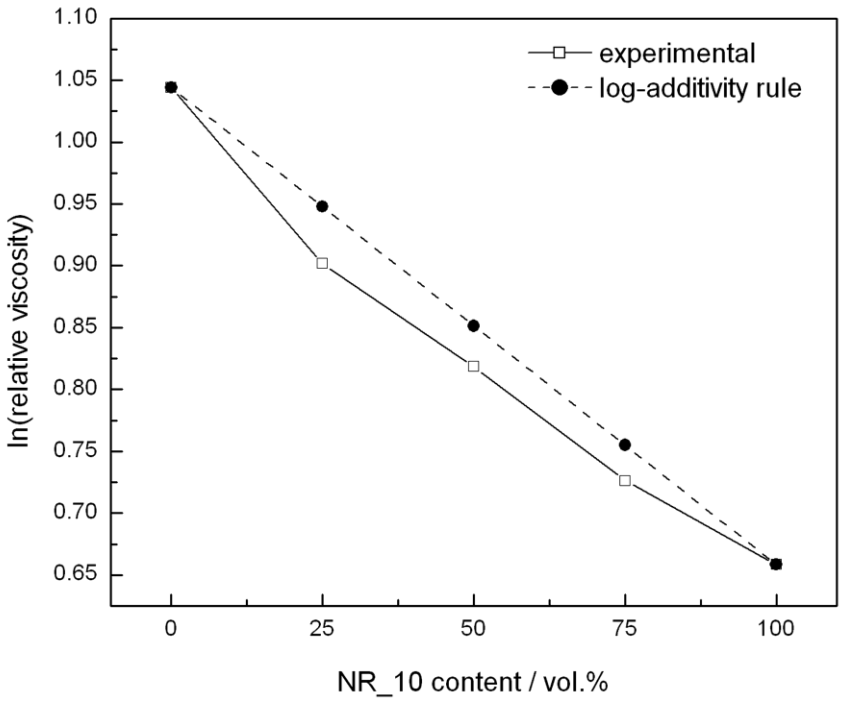

Figure 9. Comparison between experimental and theoretical viscosities for aqueous dispersions of NR_10/PVAc_10 with 2 wt.% PVOH.

of particles. These interactions are not anticipated by theoretical prediction. A number of factors can be adduced for the reduced mobility of the particles. They include repulsive forces between the mixed components because of dissimilarity in their chemical natures, as for example, NR and PVAc, and high viscosity of medium which prevent free mobility, and hence interactions between components. While the first factor might be the reason for the negative deviation observed for the pure blends of NR_10 and PVAc_10 (Figure 6), the case of negative deviations observed with the blends containing 1 and 2% PVOH (Figures 8 and 9, respectively) might be due to high viscosity of the system. In Figure 7, the introduction of 0.5% PVOH enhances freedom of intermolecular interactions between the mixed components. This increased mobility is thus observed as the positive deviation from the theoretical prediction.

Conclusions

The flow behaviours of NR latexes and PVAc dispersions, and mixtures of these dispersions, in aqueous medium, as well as the addition of a PVOH modifier to these dispersions, were investigated. The results clearly showed that changes in the relative viscosities of mixtures of NR, PVAc and PVOH dispersions are governed by a balance between the following four effects:

(i) The higher mobility of the NR chains compared to those of PVAc, which generally caused a decrease in the viscosities of the dispersion mixtures,
(ii) The physical adsorption of PVOH on the NR chains that slowed down the movement of these chains and caused an increase in relative viscosity,
(iii) The chemical interaction between the functional groups on PVAc and PVOH that gave rise to latex thickening and increased the relative viscosity,
(iv) A dilution effect which reduced the viscosity, unless counterbalanced by one or more of the other effects.

ACKNOWLEDGEMENTS

The National Research Foundation of South Africa (GUN 62693) and the University of the Free State are acknowledged for financial support of this research.

REFERENCES

Amalvy JI, Soria DB (1996). Vibrational spectroscopic study of distribution of sodium dodecyl sulphate in latex films. Progr. Org. Coat. 28:279-283.
Backman AC, Lindberg KAH (2004). Interaction between wood and polyvinyl acetate glue studied with Dynamic Mechanical Analysis and Scanning Electron Microscopy. J. Appl. Polym. Sci. 91:3009-3015.
Billmeyer FW Jr. (1984). Textbook of Polymer Science, 3rd ed.; Wiley: New York. P. 149.
Blackley DC (1966). High Polymer Latices, Vol. 2. Applied Science, London.

Brown GL, Garrett BS (1959). Latex thickening: Interactions between aqueous polymeric dispersions and solutions. J. Appl. Polym. Sci. 1:283-295.
Calvert KO (1982). Polymer Latices. Applied Science, London.
Chen J, Spear SK, Huddleston JG, Rogers RD (2005). Polyethylene glycol and solutions of polyethylene glycol as green reaction media. Green Chem. 7:64-82.
Danait A, Deshpande DD (1995). A novel method for determination of polymer-polymer miscibility by viscometry, Eur. Polym. J. 31:1221-1225.
Dibbern-Brunelli D, Atvars TDZ (1995). Study of miscibility of poly (vinyl acetate) and poly (vinyl alcohol) blends by fluorescence spectroscopy. J. Appl. Polym. Sci. 55:889-902.
Dibbern-Brunelli D, Atvars TDZ, Joekes I, Barbosa VC (1998). Mapping phases of poly (vinyl alcohol) and poly (vinyl acetate) blends by FTIR microspectroscopy and optical fluorescence microscopy. J. Appl. Polym. Sci. 69:645-655.
Geurink PJA, van Dalen L, van der Ven LGJ, Lamping RR (1996). Analytical aspects and film properties of two-pack acetoacetate functional latexes, Prog. Org. Coat. 27:73-78.
Haiyang Y, Pingping Z, Feng R, Yuanyuan W, Tiao Z (2000). Viscometric investigations on the intermolecular interactions between poly (methyl methacrylate) and poly (vinyl acetate) in various solvents, Eur. Polym. J. 36:21-26.
Haque ME, Akhtar F, Dafader NC, Al-Siddique FR, Sen AR, Ahmad MU (1995). Characterization of natural rubber latex concentrate from Bangladesh, Macromolecular Reports A32 suppl. 4:435-445.
Hellgren A, Weissenborn P, Holmberg K (1999). Surfactants in water-borne paints. Prog. Org. Coat. 35:79-87.
Hornby M, Peach J (1993). Foundations of Organic Chemistry; Oxford University Press, New York.
Hourston DJ, Hughes ID (1978). Dynamic mechanical and sonic velocity behaviour of polystyrene-poly (vinyl methyl ether) blends. Polymer 19:1181-1185.
Irving S (Ed.) (1990). Handbook of Adhesives Third Ed. Van Nostrand Reinhold, New York.
Kim S, Kim HJ (2006). Thermal stability and viscoelastic properties of MF/PVAc hybrid resins on the adhesion for engineered flooring in under heating system. ONDOL Thermochimica Acta 444:134-140.
Kosto KB, Schall DC (2007). Low-temperature waterborne pavement marking paints: a road assessment of this LOW-VOC option. Presented at the 2007 FutureCoat! Conference, sponsored by Federation of Societies for Coatings Technology, in Toronto, Ont., Canada, October 3-5, 2007.
Kuleznev VN, Melnikova OL, Klykova VD (1978). Dependence of modulus and viscosity upon composition for mixtures of polymers. Effects of phase composition and properties of phases. Eur. Polym. J. 14:455-461.
Lloyd DA (1989). A First Course in Organic Chemistry. Wiley, Chichester.
Meng W, Wu L, Chen D, Zhong A (2008). Ambient self-crosslinkable acrylic microemulsion in the presence of reactive surfactants. Iran. Polym. J. 17(7):555-564.
Nabuurs T, Baijards RA, German AL (1996). Alkyd-acrylic hybrid systems for use as binders in waterborne paints. Progr. Org. Coat. 27:163-172.
Nakamae M, Yuki K, Sato T, Maruyama H (1999). Preparation of polymer emulsions using a poly (vinyl alcohol) as a protective colloid, Colloids and Surfaces A: Physiochem. Eng. Aspects 153:367-372.
Okaya T, Tanaka T, Yuki K (1993). Study on physical properties of poly (vinyl acetate) emulsion films obtained in batchwise and in semicontinuous systems. J. Appl. Polym. Sci. 50:745-751.
Papanagopoulos D, Dondos A (1996). Difference between the dynamic and static behaviour of polymers in dilute solutions. 3. Influence of the host polymer on the dimensions of the guest polymer, Polymer 37:1053-1055.
Peethambaran NR, Kuriakose B, Rajan M, Kuriakose AP (1990). Rheological behaviour of natural rubber latex in the presence of surface-active agents. J. Appl. Polym. Sci. 41:975-983.
Sanguansap K, Suteewong T, Saendee P, Buranabunya U, Tangboriboonrat P (2005). Composite natural rubber based latex particles: A novel approach. Polymer 46:1373-1378.
Schoeder WD, Brown GL (1951). Carboranesiloxane Polymers. Rubber Age 69:433.
Singh YP, Singh RP (1983). Compatibility studies on solutions of polymer blends by viscometric and ultrasonic techniques. Eur. Polym. J. 19:535-541.
Sirisinha C, Limcharoen S, Thunyarittikorn J (2003). Oil resistance controlled by phase morphology in natural rubber/nitrile rubber blends. J. Appl. Polym. Sci. 87:83-89.
Tambe SP, Singh SK, Patri M, Kumar D (2008). Ethylene vinyl acetate and ethylene vinyl alcohol copolymer for thermal spray coating application. Prog. Org. Coat. 62:382-386.
Utracki LA, Kanial MR (1982). Melt rheology of polymer blends. Polym. Eng. Sci. 22:96-114.
Wong ACY (1991). The Study of the Relationships Between Melt Index, Density abd Blend Ratio of Binary Polyethylene Blends. Polym. Eng. Sci. 31(21):549.
Yip E, Cacioli P (2002). The manufacture of gloves from natural rubber latex. J. Allergy Clin. Immunol. 110:S3-S14.
Zhaoying Z, Yuhui H, Bing L, Guangming C (2001). Studies on particle size of waterborne emulsions derived from epoxy resin. Eur. Polym. J. 37:1207-1211.

academicJournals

Vol. 8(31), pp. 1597-1601, 23 August, 2013
DOI: 10.5897/IJPS2013.3998
ISSN 1992 - 1950 © 2013 Academic Journals
http://www.academicjournals.org/IJPS

International Journal of Physical Sciences

Full Length Research Paper

Synthesis, structural and optical characterizations of cadmium oxide (CdO) thin films by chemical bath deposition (CBD) technique

B. A. Ezekoye[1]*, V. A. Ezekoye[1], P. O. Offor[2] and S. C. Utazi[1]

[1]Crystal Growth and Characterization Laboratory, Department of Physics and Astronomy, University of Nigeria, Nsukka, Enugu State, Nigeria.
[2]Department of Metallurgical and Materials Engineering, University of Nigeria, Nsukka, Enugu State, Nigeria.

Accepted 15 August, 2013

Thin films of cadmium oxide (CdO) were synthesized and characterized using chemical bath deposition (CBD) technique. The XRD studies revealed amorphous CdO thin films which upon annealing at 623K transformed to polycrystalline structure. The optical studies showed that the CdO films have high average transmittance over 60% in the visible region and direct optical bandgaps of 2.02 ± 0.05 eV, 2.03 ± 0.05eV and 2.05 ± 0.05eV for samples X, Y, Z respectively. These characteristics make them good candidates for applications in photodiodes, phototransistors, photovoltaics, transparent electrodes, liquid crystal displays, IR detectors and anti-reflection coatings.

Key words: Thin films, chemical bath method, cadmium oxide, characterizations, bandgap.

INTRODUCTION

Metallic oxides are becoming prominent and important group of materials due to their versatile physiochemical, structural, and optical characteristics which include high temperature superconductivity, ferroelectricity, ferromagnetism, piezoelectricity, semiconductivity, optical, opto-electronic, magnetic, electric, thermal, electrochemical, catalytic and sensor properties (Jia et al., 2004; Vayssieres, 2004). Other attractive optical properties are low bandgap, high transmission, coefficient, invisible spectral domain, remarkable and luminescence characteristics (Ortega et al., 1999; Rusu and Rusu, 2005). The diversity emanates from the more complex crystal and electronic structures of metal oxides in comparison to other classes of materials. The elegancy of the metal oxides are found in the oxidation states, coordination numbers, symmetry, crystal-field stabilization, density, stoichiometry and acid-base surface properties that they exhibit. These characteristics made them to find applications in photodiodes, phototransistors, photovoltaics, transparent electrodes, liquid crystal displays, IR detectors and anti-reflection coatings (Dhawale et al., 2008).

The cadmium oxide (CdO) thin films are n-type semiconductor that exhibits rock salt structure (FCC) with wide optical bandgap of 2.2 eV, high conductivity and high transmission in VIS region (Ortega et al., 1999; Henriguez et al., 2008). The thin films have attracted attention in recent years due to their attractive properties and wide range of technical applications in transparent electrodes, photovoltaics and display devices, saucers and others (Dhawale et al., 2008). The films also have been used as transparent contact in CuInSe2 and Si Solar Cells (Ortega et al., 1999).

Different techniques have been used by researchers in the past ten years for synthesizing the thin films such as spray pyrolysis, sputtering, pulsed laser deposition,

*Corresponding author. E-mail: benjamin.ezekoye@gmail.com.

sol-gel spin coating, electrochemical, activated reactive evaporation, metal organic chemical vapour deposition (MOCVD) and chemical bath method or solution growth methods (Henriguez et al., 2008; Caglar and Yakuphanoglu, 2009). In this study chemical bath method (CBD) was used in synthesizing cadmium oxide (CdO) and the synthesized samples were characterized using XRD, SEM and UV-VIS spectrophotometric techniques in order to find their possible areas of applications.

MATERIALS AND METHODS

The starting chemicals used in this work without further purification include cadmium chloride ($CdCl_2.4H_2O$) (AR chemicals grade), ammonia ($NH_3.H_2O$) and double distilled water (DDW). PVA and PVP cadmium chloride ($CdCl_2.4H_2O$) was used as precursor for the preparation of CdO thin films as a Cd^{2+} ionic source.

A detail of chemical bath deposition (CBD) has been discussed elsewhere (Ezekoye and Okeke, 2006; Ezema and Osuji, 2008). Stock solution (5 ml) of $CdCl_2$ was poured in a beaker followed by addition of 4 ml of 30% NH_3, with slight shake gave a whitish solution which is odourless. More of 30% NH_3 was poured into the set-up until it was clear by a total of 4 ml of NH_3. Double distilled water (H_2O, 34 ml) was added to the set-up which gave a fair whitish colour. The set-up was kept into an open conical flask where a good amount of oxygen was sufficiently supplied to it. A whitish film was deposited on the glass slide after 45 h, which turned clearly whitish when rinsed with distilled water.

Sample Y was post-treated at 200°C for 1 h which gave a whitish colour after the annealing. Sample X was post-treated at 400°C for 1 h, forming a brownish colour after the annealing. Sample Z was as-deposited, that is, no treatment given.

For the complex formation, an excess ammonium hydroxide solution (NH_3+H_2O) was added (30%) till a clear solution was obtained. The clear solution was kept under unstirred condition and glass substrate was dipped in it for 45 h. Whitish films due to the $Cd(OH)_2$ were formed on glass substrate. The CdO films were annealed in oxygen air-tight container at 473 and 673K for 1 h which generally facilitates decrease in dislocations, stresses, and inhomogeneities (Dhawale et al., 2008). The change in colour from whitish to brown films during annealing confirmed the formation of CdO. The equations for the reactions are as follows:

$$CdCl_2 + NH_3 + H_2O \longrightarrow [Cd(NH_3)_4]^{2+} + 2OH^- + 2Cl^- \quad (1)$$

$$2OH^- + Cd^{2+} \longrightarrow CdO + H_2O \quad (2)$$

RESULTS AND DISCUSSION

Thickness measurement

Film thickness (d) was determined by gravimetric weight difference method using high precision electronic balance given by the relation (Ezekoye and Okeke, 2006):

$$d = \frac{M}{(\rho \; x \; A)} \quad (3)$$

where M is the mass of the film deposited on the substrate in gram, A is the area of the deposited film and ρ, the density of the deposited material. The maximum thickness obtained for CdO thin film was 180 *n*m. This thickness is greater than the nano range classification of materials.

Optical studies

Optical properties of cadmium oxide (CdO) thin films were investigated by UV–VIS spectrophotometric technique. The absorption coefficient(α) is related to incident photons by the relation $\alpha h\nu = A(h\nu - E_g)^n$ (Caglar and Yakuphanoglu, 2009; Ezema and Osuji, 2008; Mohamed and Ali, 2008), where *A* is a constant and *n* is an index that characterizes the optical absorption process and is theoretically equal to 1/2, 2, 3/2 and 3 for direct allowed, indirect allowed, direct forbidden and indirect forbidden transitions, respectively. Since CdO is a direct band gap semiconductor, the $(\alpha h\nu)^2$ versus the $h\nu$ diagram is depicted in Figure 1. The straight line on the curve at horizontal axis shows the energy band gap of the CdO thin films and is corresponding to 2.02 ±0.05eV (Sample Z) for the as-grown film. By annealing at 200 and 400°C, the band gap increased to 2.03 ± 0.05eV (Sample Y) and 2.05 ± 0.05eV (Sample X), respectively.

Figure 2 shows absorption spectra of CdO. The variation of optical absorbance (α) with wavelength (λ) of CdO film is shown in Figure 2. These spectra reveal that as-grown CdO films have low absorbance in the visible region. Figure 3 shows the transmittance spectra for CdO films. The increase in transmittance with increasing wavelength in ultra-violet (UV) region is fairly sharp. The absorption coefficient (α) was determined from the relation, $\alpha = \left(\frac{1}{d}\right)\ln\left(\frac{1}{T}\right)$, where d is the thickness of the film and T is the transmittance (Caglar and Yakuphanoglu, 2009; Mohamed and Ali, 2008) (Figure 3). This indicates that the absorption band gap transitions, which is characteristic of CdO and the fundamental absorption, which corresponds to electron excitation from the valence band to conduction band can be used to determine the nature and value of the optical band gap. The optical studies showed that the CdO films have high average transmittance over 60% in the visible region.

Film structure

Figures 4 (X), 4 (Y) and 4 (Z) show the XRD spectra of the grown CdO thin films. The film structure was studied by X-ray diffraction (XRD) technique using the CuK_α a radiation (λ = 0.1790 nm) and the grain size or crystallite size D was obtained using the Debye Scherrer relation (Barman et al., 2005):

$$D_{hkl} = \frac{K\lambda}{\beta \cos\theta}, \quad (4)$$

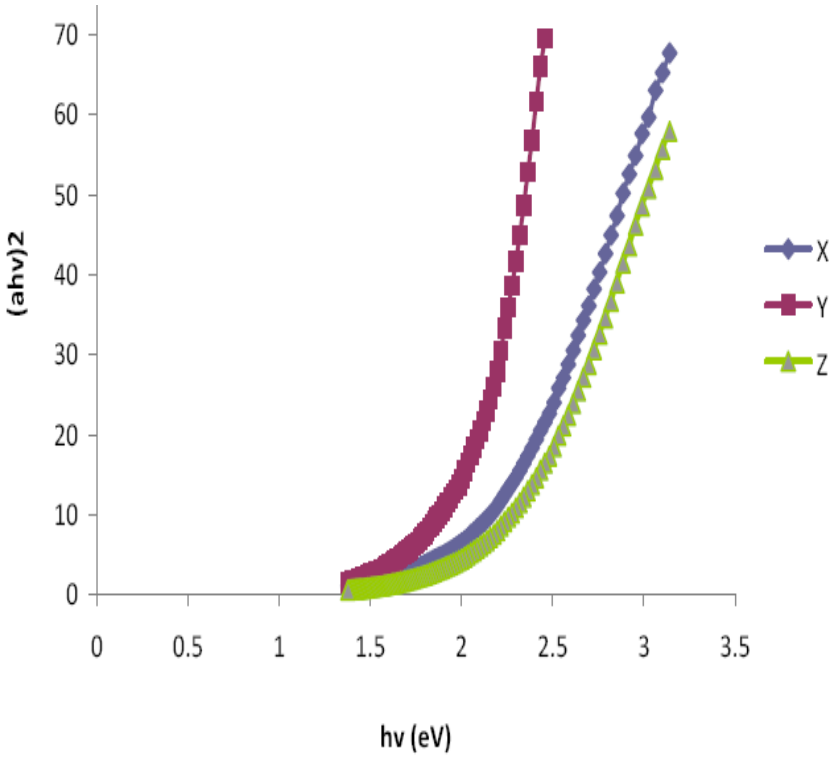

Figure 1. Plot of $(\alpha h\nu)^2$ against photon energy $h\nu$ (eV).

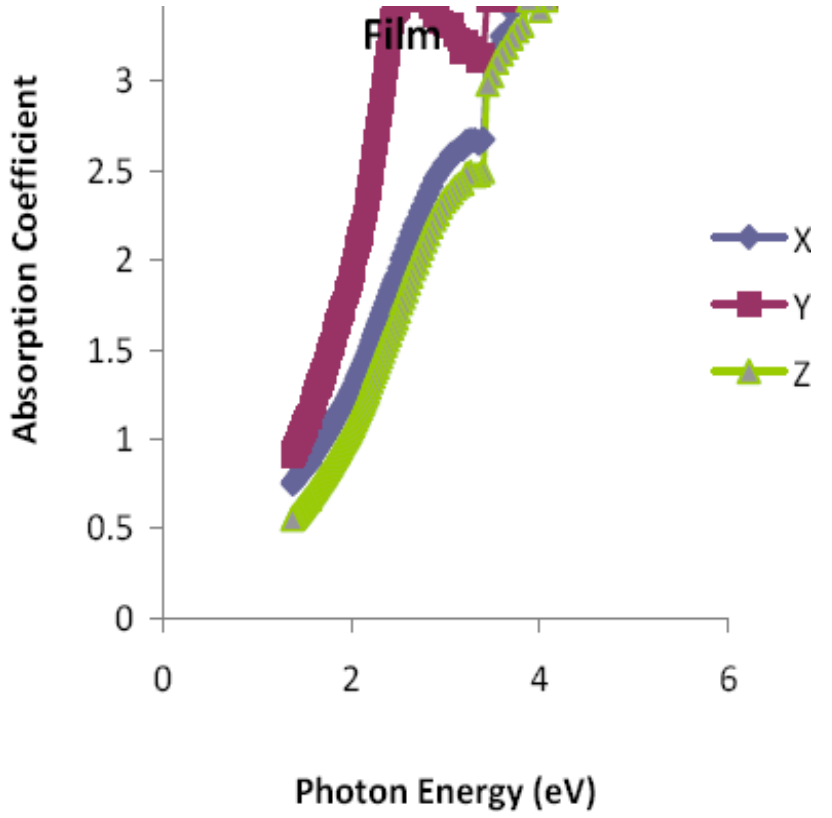

Figure 2. Plot of absorption coefficient against photon energy hv (eV).

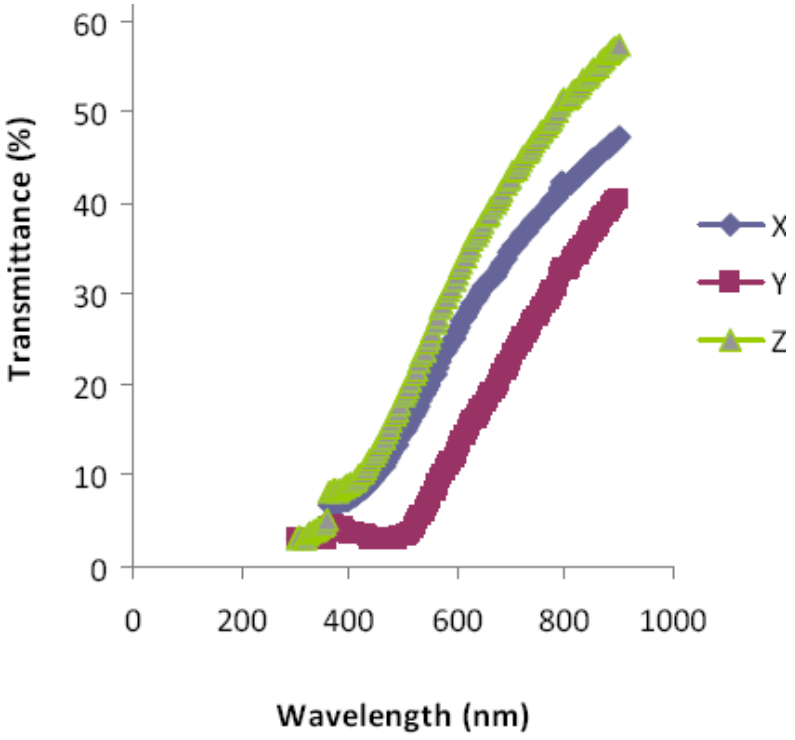

Figure 3. Plot of Transmittance (%) against photon energy h ν (eV).

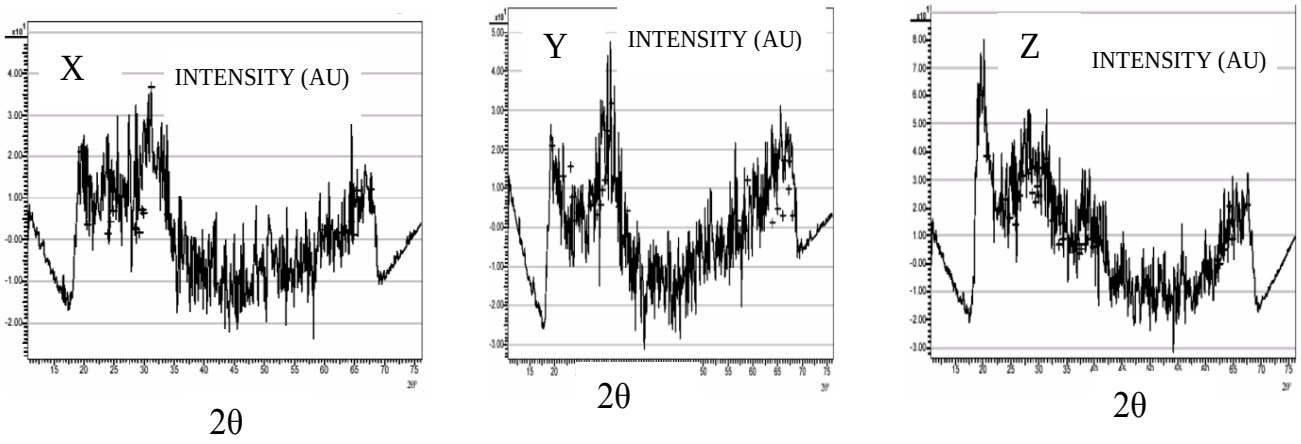

Figure 4. XRD spectra of the cadmium oxide thin film (X) annealed at 400°C (Y) annealed at 200°C and (Z) as-grown.

where K = 0.94, is the shape factor, $\lambda = 15408\text{Å}$, θ is the diffraction peak angle (Bragg's angle) in degrees and β is the full width at half maximum (FWHM) in radians, of the corresponding diffraction peak. Table 1 shows the various parameters of the grown film at 298, 473 and 673K. By increasing the annealing temperatures, the grain size of the crystallite was found to increase which is in agreement to Barman et al. (2005). Figure 5 shows the micrographs of the as-grown films (Z), and the annealed at 200°C (Y) and annealed at 400°C (X). The as-grown is amorphous while the annealed became crystalline as can be seen by increase in grain-size in Table 1.

Conclusion

Thin films of cadmium Oxide (CdO) were synthesized and characterized using CBD technique. The XRD

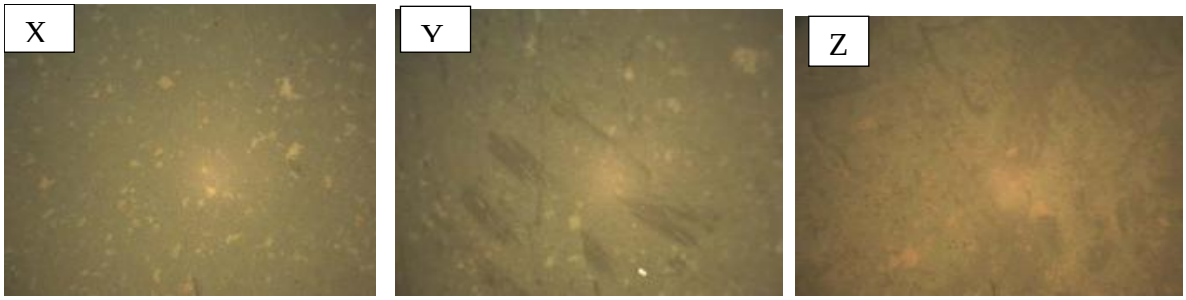

Figure 5. SEM image of samples X, Y, Z of the cadmium oxide thin films.

Table 1. XRD Parameters of the grown cadmium oxide (CdO) thin films.

Sample	Peak type	Peak position	Grain size (nm)	FWHM (°)	Bandgap (eV)
Z(278K)	(111)	31.19	28.675	1.4259	2.05 ± 0.05
Y(473K)	(111)	30.11	29.6749	0.96616	2.03 ± 0.05
X(673K)	(111)	20.64	43.0241	0.78548	2.02 ± 0.05

studies revealed amorphous CdO thin films which upon annealing at 623K transformed to polycrystalline structure. The optical studies showed that the CdO film has a high average transmittance of about 60% in the visible region with presence of direct bandgaps values of 2.02 ± 0.05eV, 2.03 ± 0.05eV and 2.05 ± 0.05eV for samples X, Y, Z, respectively. These characteristics make them good candidates for applications in photodiodes, phototransistors, photovoltaics, transparent electrodes, liquid crystal displays, IR detectors and anti-reflection coatings.

REFERENCES

Barman J, Borah JP, Sarma KC (2005). Synthesis and Characterization of CdS Nanoparticles by Chemical Growth. Optoelectronic Adv. Mater. Rapid Commun. 2(12):770-774.

Caglar M, Yakuphanoglu F (2009). Fabrication and Electrical Characterization of Flower-like CdO/p-Si Heterojunction Diode. J. Phys D: Appl. Phys. 42(045102):5.

Dhawale DS, More AM, Latthe SS, Rajpure KY, Lokhande CD (2008). Room Temperature Synthesis and Characterization of CdO Nanowires by Chemical Bath Deposition (CBD) Method. Appl. Surf. Sci. 254:3269-3273.

Ezekoye BA, Okeke CE (2006). Optical Properties in PbHgS Ternary Thin Films Deposited by Solution Growth Method. Pac. J. Sci. Technol. 7(2):108-113.

Ezema FI, Osuji RU (2008). Preparation and Optical Properties of Chemical Bath Deposited MnCdS2 Thin Films. *FIZIKA A (Zagreb)*. 16(2):107-116.

Henriguez R, Grez P, Munoz E, Lincot D, Dalchiele EA, Marotti R, Gomez H (2008). One-step Pentiodynamic Synthesis of Polycrystalline Cadmium Oxide (CdO) Thin films in DMSO Solution. Sci. Technol. Adv. Mater. 9:025016.

Jia QX., Mccleskey, TM, Burrell AK, Collis GE, Wang H, Li ADQ, Foltyn SR (2004). Polymer-assisted Deposition of Metal Oxide Films. Nature Materials. 3: www.nature.com/naturematerials.

Mohamed HA, Ali HM (2008). Characterization of ITO/CdO/Glass Thin Films Evaporated by Electron Beam Technique. Sci. Tech. Adv. Mater. 9(025016):9.

Ortega M, Santana G, Morales-Acevedo A (1999). Optoelectronic Properties of CdO-Si Heterojunctions. Superficies y Vacio. 9:294-295.

Rusu RS, Rusu GI (2005). On the Electrical and Optical Characteristics of CdO Thin Films. J. Optoelectronics Adv. Mater. 7(2):823-828.

Vayssieres L (2004). On the Design of Advanced Metal Oxide Nanomaterials. Int. J. Nanotechnol. 1(1/2):6-8.

UPCOMING CONFERENCES

International Conference on Mathematical Modeling in Physical Sciences Prague, Czech Republic, September 1-5, 2013

14th International Conference on Accelerator and Large Experimental Physics Control Systems. The Hyatt Regency Embarcadero Center San Francisco, California October 6-11, 2013

Conferences and Advert

September 2013
International Conference on Mathematical Modeling in Physical Sciences
Prague, Czech Republic, September 1-5, 2013

October 2013
14th International Conference on Accelerator and Large Experimental Physics Control Systems. The Hyatt Regency Embarcadero Center San Francisco, California October 6-11, 2013

International Journal of Physical Sciences

Related Journals Published by Academic Journals

- *African Journal of Pure and Applied Chemistry*
- *Journal of Internet and Information Systems*
- *Journal of Geology and Mining Research*
- *Journal of Oceanography and Marine Science*
- *Journal of Environmental Chemistry and Ecotoxicology*
- *Journal of Petroleum Technology and Alternative Fuels*

academicJournals